

Department of Precision and Microsystems Engineering

Development of a stretchable graphene electrode for an electrochemical cell

Manuel Adrián Estrada

Report no : MNE 2016.020
Coach : Dr.ir. Luigi Sasso
Professor : Prof.dr. Urs Staufer
Specialisation : Micro and Nano Engineering
Type of report : Master of Science Thesis
Date : October 2016

The truth knocks on the door and
you say, "Go away, I'm looking for the
truth," and so it goes away.

*Zen and the art of motorcycle
maintenance*
Robert M. Pirsig

Abstract

Strain engineering has been shown to alter the electronic properties of graphene, thereby changing its chemical reactivity. If this change in reactivity can be used to improve the adsorption of species on its surface, the exceptional properties of graphene can improve current sensing capabilities. The graphene surface could be functionalised such that it can act as a basis material for a new generation of small-scale, hypersensitive and low-power sensors. These can be unobtrusively incorporated in everyday items; a futuristic forecast, as described in the *Internet of Things*. However, how can this strain be achieved and how can we map the change in chemical activity? In this thesis, methods are developed in which the electroactivity of graphene can be measured while it is being strained. Graphene grown by chemical vapour deposition was transferred to a flexible, insulating substrate and strain -applied to the substrate- was transferred to the material, as measured with Raman spectroscopy. An electrochemical setup has been built that is able to use graphene as electrode material on which a electrolyte-containing solution is present in the form of a droplet.

Acknowledgements

I would like to thank the following people, who have helped me, directly or indirectly, in realising this document and all the work that was required.

Luigi Sasso, whom I asked to be my daily supervisor half-way in the project; his calm and kind personality matched perfectly with a chaotic and turbulent person such as myself. Urs Stauer, whose analytical mind helped tremendously in opening new doors and broadening my perspective. Yexian Wu, who was my daily supervisor in the first half of the project and pushed me in the right direction during the initial phase of the project.

Being in a university environment, especially in the department of Precision and Microsystems Engineering, gives you the advantage that you're surrounded by many highly intelligent people and I tried to use this to my advantage as much as possible. I would like to thank Alkisti Gkouzou, Eleonor Verlinden, Jaap Kokorian and Cristina Varone, at whose door I knocked numerous times like a younger sibling: they were always willing to help, despite their own busy schedules. They've helped me a lot in gaining new insights and their competences have shown me that there is much for me to learn. On a darker note, their access to free coffee has deteriorated my coffee addiction to a point of extremal tremors. Also Paola Fanzio fits in this group, who helped me in the lab and introduced me to transparent polymer materials, which have become an important part of my research. When talking about academic stimulation, I cannot forget Murali Ghatkesar. Murali has an incredible curiosity and a real passion for science; I would not be able to count the times he has helped me in my research. Furthermore, Guido Janssen for his expertise and wisdom regarding CVD graphene and Menelaos Tsigkourakos for his help with Raman spectroscopy.

Outside of our department, Sten Vollebregt from the Else Kooi Laboratory, the *deus ex machina* who provided me with batches of CVD graphene, free of cost, without whom I probably would have had to resort to the black market. Yaiza Gonzalez-Garcia, for being willing to help me, initially with the idea of using electrochemical microscopy (which I unfortunately didn't get around to), later for accepting my request to be in my thesis committee. Also thanks to Agnieszka Kooijman, like Yaiza from the department of Materials Science and Engineering, for showing me their lab and experimental setups.

The technical staff, Rob Luttjeboer, Harry Jansen and Patrick van Holst, without their

practical expertise I couldn't have done this project.

A tremendous help, academically and personally speaking, has been Bram Sterke, the few times that he helped me turned out to have huge consequences, in a positive way, which must be the effects of being a wonderful person all-around. Also thanks to Melle van Overbeek, Thomas Ponds and Maartje de Boer for supporting me and putting up with me all this time.

I have been blessed with the most luxurious offices ever seen in the history of graphene electrochemistry at the department of Micro and Nanoengineering at the TU Delft, but I've been even more lucky with my room mates and study colleagues who've had to listen to my rambling and were able to stay level-headed. In particular I would like to thank Tijn van Omme, who has helped me with too many things to list here, but most of all, prevented me in doing even more things. Sarah Aalbers, Pooya Motthagi, Michiel Dondorp, Rolf Swuste, Mahesh Prasad, Jimmy Schoubroeck, Jan Willem Feitsma, Michael Mengolini, Rick de Gruiter, Thijs Smit, Rahul Rahul Rahul, Ryan van Dommelen, Leroy Boerefijn: thank you for making the past 'year' highly enjoyable.

Lastly, I would like to thank my family for their support, trust, patience, and, above all, unconditional love.

Contents

Preface and acknowledgements	vii
1 Introduction	1
1.1 Industry scope	1
1.2 Graphene in a sensor	3
1.3 Research goals	3
1.4 Project outline	4
2 Theory	5
2.1 Introduction to graphene	6
2.2 Production methods	7
2.3 Strained graphene	11
2.4 Electrochemistry of graphene	15
2.5 Conclusion	20
3 Design of an experimental setup for electrochemistry in a drop	21
3.1 Introduction	21
3.2 Cyclic voltammetry	21
3.3 Graphite CV	24
3.4 Graphene CV	26
3.5 Summary and conclusion	29
4 Design and production of a stretchable graphene electrode	31
4.1 Introduction	31
4.2 Intermission: issues regarding uniaxial strain with a tensile MEMS	32
4.3 Materials and methods	33
4.4 Results and discussion	38
4.5 Summary and conclusion	47
5 Conclusions and recommendations	49
5.1 Conclusions	49
5.2 Outlook	50
A Electrochemistry basics	57

B	Ag/AgCl reference electrode preparation	61
C	Additional photos of CV experimental setup	65
D	Results of the relaxed graphene CV	67
E	Design of a micro-electrochemical cell	71

at Colby College, Maine, speaking to Business Week, expanded:

"In the next century, planet earth will don an electronic skin. It will use the Internet as a scaffold to support and transmit its sensations. This skin is already being stitched together. It consists of millions of embedded electronic measuring devices: thermostats, pressure gauges, pollution detectors, cameras, microphones, glucose sensors, EKGs, electroencephalographs. These will probe and monitor cities and endangered species, the atmosphere, our ships, highways and fleets of trucks, our conversations, our bodies—even our dreams."[18]

Today, the IoT can be found in daily life in the form of thermostats, lighting and wearable electronics and if the present trend continues it would soon be easier to list things that are *not* part of the IoT. Regardless of the ultimate implementation of this novel idea, it is clear that there is a need for small, precise and power-efficient sensors.

A sensor is able to detect a physical phenomenon and output this appropriately. Often this output is in the form of an electrical signal; one can think of a piezoceramic strain gauge or a temperature sensor on a CPU. Often they are used in digital systems where an event or change in environment has to be measured, in which case a change in resistance is the output. An ideal sensor is able to detect the smallest amount of change: this can be distinguished into a minimum threshold and a maximum sensitivity as objective.

In fact, the demand and possibilities of small, sensitive sensors is far greater than in the IoT. In nature for instance, micro-sized sensors are already found and are able to detect -for example- molecules or enzymes, which is something that scientists are unable to mimic (for now). The scale at which engineering is done is decreasing dramatically and as sensors are the only window for observation of the physical world, they should shrink accordingly.

In case of a chemical sensor, the theoretical sensitivity and threshold limit is one atom or molecule. Current sensors are unable to approach this limit due to intrinsic electrical noise overshadowing the electrical change from individually detected molecules[53]. This noise limits the performance of other types of sensors too and graphene seems to be highly appropriate to tackle this problem. Graphene is exceptionally conductive, exhibiting a room-temperature mobility of $\sim 10\,000\text{ cm}^2\text{V}^{-1}\text{s}^{-1}$ [39]. This means that a small number of extra electrons can already cause a notable change in carrier concentration, allowing for a high sensitivity, which makes it a extremely promising candidate as a sensor material.

1.2 Graphene in a sensor

Since the Nobel Prize winning experiments of Andre Geim and Konstantin Novoselov[39] in 2004 a plethora of research has been done on the two-dimensional material graphene. Despite it being difficult to be seen outside of a laboratory setting, scientists have high hopes for this unique material.

One of these hopes is the use of graphene as a transducer in sensors. After being modified, its low resistivity could provide low-power and low-threshold sensing and its large specific surface area immensely reduces the possible sensor size. One can dream of sensors that are small and efficient enough to be incorporated in a pill, band-aid or sticker that would fit perfectly into a world where engineering is found in ever-decreasing dimensions.

In order to find out if graphene can be used in a sensor, first it should be investigated if it can be functionalised such that it is able to detect a signal or stimulus, e.g., a functional group is bound to the graphene surface, causing its resistance to change when the group detects a certain condition. The process of modifying a solid conducting substrate is often referred to as electrografting[4]. Unfortunately, due to its electronic structure, pristine graphene displays little chemical activity which makes covalent bonding a difficult process[1]. These days, nano-engineers are trying to attain the exceptional sensing possibilities of graphene by producing graphene oxide out of graphite[28][64][27], which is much more practical for high-volume and large-scale production but paid off greatly with a decrease in measurement precision and effectiveness.

Fortunately, research shows that the chemical activity of pristine graphene can be affected by tensile stress. By increasing the physical distance between the carbon atoms its electronic structure can be altered which could be beneficial to the bonding of functional molecules[1][7].

Now, from the theses above, the question arises: *How can the straining of graphene can improve its readiness to being modified with functional groups, which could contribute to the realisation of next generation sensing?*

1.3 Research goals

The research goal is to find out whether straining graphene can improve its readiness to accept covalent bonds in order to facilitate surface modification. Surface modification is often carried out through electrochemistry: in an electrochemical cell electrons are transferred between an electrode and an oxidation-reduction reaction at the Helmholtz layers. Analogously, in a covalent bond they are transferred between the free species and a shared electron pair. The focus of this research will not be on which types of functionalisation species would be suited for specific applications, but rather a preliminary investigation on how the electrochemical properties of graphene change due to

strain. Considering this, the research goal is translated into the main research question as follows:

How does strain influence the electrochemical properties of graphene?

1.3.1 Thesis hypothesis

The straining of graphene can improve its chemical reactivity which makes it easier to attach molecules to its surface with covalent bonds, thus making it easier to functionalise the surface, which is necessary to make graphene-based sensors.

1.4 Project outline

This document will start with the theoretical background to the problem at hand and provides an analysis which will form the backbone for the rest of the project, in Chapter 2. Included in this chapter are the past researches done regarding strain engineering of graphene and graphene electrochemistry. With this knowledge in mind, first, an experimental setup is designed and built that is able to do electrochemical measurements in a droplet, in Chapter 3. Next, the design and development of a stretchable graphene is described in Chapter 4. Finally, the conclusions of these chapters will be summarised in the final chapter, along with an outlook that shows a vision that builds on the research described in this document.

Furthermore there are five appendices: Appendix A gives some background information about electrochemistry, Appendix B contains a description of the production of the Ag/AgCl electrode used in Chapter 3. Appendix C shows the setup used for the Graphite CV, Appendix D has some extra graphs supporting Chapter 2.4 and Appendix E contains a basic description of the planned electrochemical experiment that was not performed in the end.

2 Theory

Up until now, graphene-based sensors generally involve chemical processes using strong acids and oxidisers to chemically produce reduced graphene oxide out of graphite[64]. Unfortunately, this greatly impairs the exceptional electronic properties of pristine graphene[8]. Graphene of the best quality is produced through mechanical exfoliation, but for larger areas ($>100\ \mu\text{m}$) chemical vapour deposition is more suited, but again paid off in terms of material quality. A short introduction into graphene and its production methods can be found in Section 2.1.

Ideally, one would want to functionalise a pristine surface of graphene with the species in question. For instance, in the case of a humidity sensor, the functional groups bind to water molecules in the air, thereby changing the resistance of the functionalised graphene, which can be measured when integrated in a circuit. A higher (electronic) quality of graphene meaning a lower limit of sensitivity and a higher signal-to-noise ratio.

Normally graphene has a reputation for being inert but fortunately, straining it could lead to a higher reactivity. Why this is the case, and how strain can be achieved will be described in Section 2.3

Electrografting is the technique to modify a conductive surface with organic groups which has good prospects of achieving robust, well-defined structures and could lead to a powerful method to make sensors and biosensors[49]. This requires the graphene to be used as an electrode in an electrochemical system. Past investigations on the electrochemical properties of graphene will be discussed in Section 2.4.

The intention in this chapter is to form a knowledge basis for this masters' thesis, after which it can be applied to form hypotheses, which, in turn will create the basis for an experimental set-up that should help to answer the research questions. The chapter is concluded in section 2.5, at which moment enough information should be collected to design the experiments needed to find out the answer to the research question.

2.1 Introduction to graphene

Graphene is a material whose existence has been known of for some decades[61] but the recent isolation and characterisation by Andre Geim and Konstantin Novoselov has sparked a tremendous interest in this material. According to the International Union of Pure and Applied Chemistry, it is (...) *A single carbon layer of the graphite structure, describing its nature by analogy to a polycyclic aromatic hydrocarbon of quasi infinite size.*[34]. Graphene is the thinnest material known to man[46] and has other unique features which have never been seen before in any material in the world, like high mechanical strength[39], high thermal conductance and an extremely high charge carrier mobility[40]. Because of these properties, it has a unequivocally promising future in applications like flexible transparent conductors, integrated circuit elements, high-frequency transistors, ultracapacitors, battery electrodes, desalination membranes, passivation layers and composite materials[11]. Graphene has already proven its benefits in the form of carbon nanotubes, which in essence are rolled up layers of graphene that are used in applications like atomic force microscopy and composite materials.

2.1.1 Electronic structure

Pristine graphene is a bonded carbon atom structure, arranged in a hexagonal ‘honeycomb’ lattice with a thickness of one atom. Each atom is connected to three other carbon atoms, forming angles of 120° ; this symmetry is a direct consequence of the electrostatic repulsion between the particles. Because of this shape, graphene has two distinct crystallographic edge directions; zigzag and armchair, as can be seen in Figure 2.1.

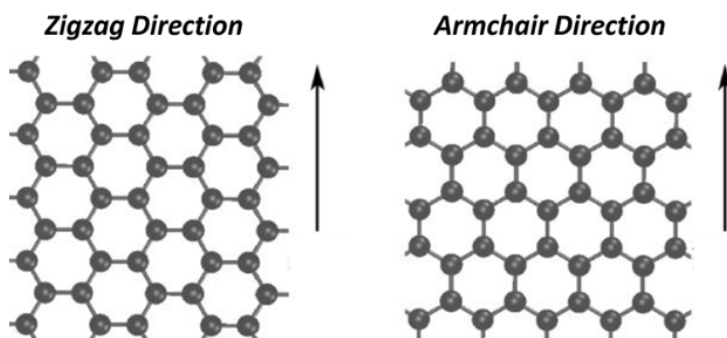


Figure 2.1: Crystallographic edge directions[46]

Graphene has some remarkable properties and most of them can be understood by studying its electron configuration. A carbon atom has four valence electrons and in the case of a graphene structure three covalent σ -bonds are present, which are hybridisations of one $2s$ orbital mixed with two of the $2p$ orbitals, resulting in sp^2 orbitals. They link the carbon atoms and are responsible for the exceptional mechanical strength and high

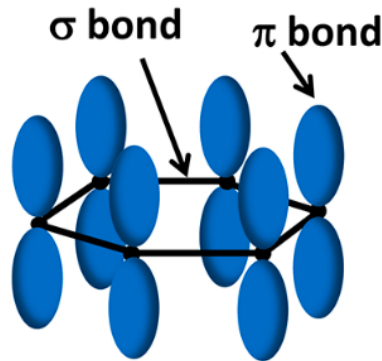


Figure 2.2: Schematic representation of the σ - and π -bonds[46]

elasticity of graphene. The fourth valence electron yields a so-called π -bond and does not contribute to the covalent bond formation. It has the unique feature of having zero band gap: this allows ballistic transport of the electrons. Per carbon atom, one electron is allocated in the π -bond and their orbitals overlap, resulting in the hopping of electrons between the different carbon nuclei. They are responsible for the high thermal and electrical conductivity of graphene, while rendering it chemically relatively inert[46][1]. More details on the π bonds can be found in Section 2.3. A visual representation of the σ - and π -bonds of a graphene unit hexagon can be found in Figure 2.2.

2.2 Production methods

Procuring graphene might seem like an easy task; you can most likely find some in every ordinary pencil. However, its properties can only be observed when it is in free-standing form and this obstacle has kept it a dormant, ‘academic’ material for many decades. The recent explosion of research was caused by the experiments of Andre Geim and Konstantin Novoselov in 2004 when they unexpectedly isolated it[39]. They used nothing more than a block of graphite, ordinary Scotch tape and a silicon wafer and for their subsequent experiments they were awarded the Nobel prize of Physics in 2010. This simple production method was a prerequisite for the current ongoing research and though their method has not changed significantly for isolating single mono-layer crystals of graphene, another method has been gaining interest since 2008. In fact, chemical vapour deposition (CVD) has become increasingly popular for the production of large, multi-crystal graphene sheets. A third large-scale method to synthesise graphene is the chemical exfoliation of graphite oxide.

In the following paragraphs these three production methods are studied. The implications of these methods within the scope of this research will be assessed in Section 2.4.

2.2.1 Mechanical exfoliation

Mechanical exfoliation requires a block of highly oriented pyrolytic graphite (HOPG) which contains highly aligned graphite crystallites and could be seen as millions of layers of graphene. Adhesive tape is used to remove a few layers which are transferred to a silicon wafer and after removing the tape, some graphite and graphene flakes stick to the wafer because of Van der Waals forces. Inspection by optical microscope is done to locate few-layer flakes and Raman spectroscopy is used to confirm the amount of layers[39]. There are a few ways for further transferring, depending on the next experiment or application. The process is illustrated in Figure 2.3, further details are left out of this document for reasons of brevity.

Advantages of this method are its simplicity and the high quality of flakes obtained; large single grain graphene flakes can be exfoliated with relatively simple tools. The main drawback is the maximum size that can be obtained; until recently, the size of an exfoliated monolayer was about $20 \times 20 \mu\text{m}$, newer techniques are reported to be in the range of $100 \mu\text{m}$ [20]. The extremely small size increases the difficulty of handling and defines experimental set-ups greatly. Another disadvantage is the lack of control over the size, the number of single-layer crystals and the random locations where they are found on the silicon substrate. It might seem that this makes this method unreliable, but because due to the high number of flakes transferred to the silicon, monolayer or few layer graphene will be found most cases. Mechanical exfoliation appears to be far from ideal in terms of scaling and reproducibility but not yet matched in terms of quality.

2.2.2 Chemical vapour deposition

In order to circumvent some of the difficulties and limitations associated with the mechanical exfoliation of graphene, scientists have started to experiment with a technique called chemical vapour deposition (CVD), which is a bottom-up approach to synthesise graphene. First reports of this technique have been published already in the late sixties[36][16] but were picked up in 2004 after a long hiatus. Generally, a carbon-containing gas mixture is led along a metal catalyst surface at high temperatures. A reaction occurs that causes some ‘pioneer’ carbon atoms to attach to certain locations on the substrate (so-called nucleation sites) after which other carbon atoms bond to the pioneers. This is often referred to as the ‘growing’ of graphene. A visualisation of this growth process is shown Figure 2.4.

As opposed to mechanically exfoliated graphene, the size of the graphene film produced can reach centimetre-lengths[25] and is much more suitable for scaling. However, the location and number of nucleation sites are hard to control which makes the film look like a patchwork quilt, which has consequences for its mechanical, electrical and chemical properties (Section 2.4.3). In some cases, nucleation sites appear on top of a previously grown layer, resulting in bilayer patches, this seems to depend on the manufacturer. In other words, the production process is reliable in terms of large-area monolayer graphene,

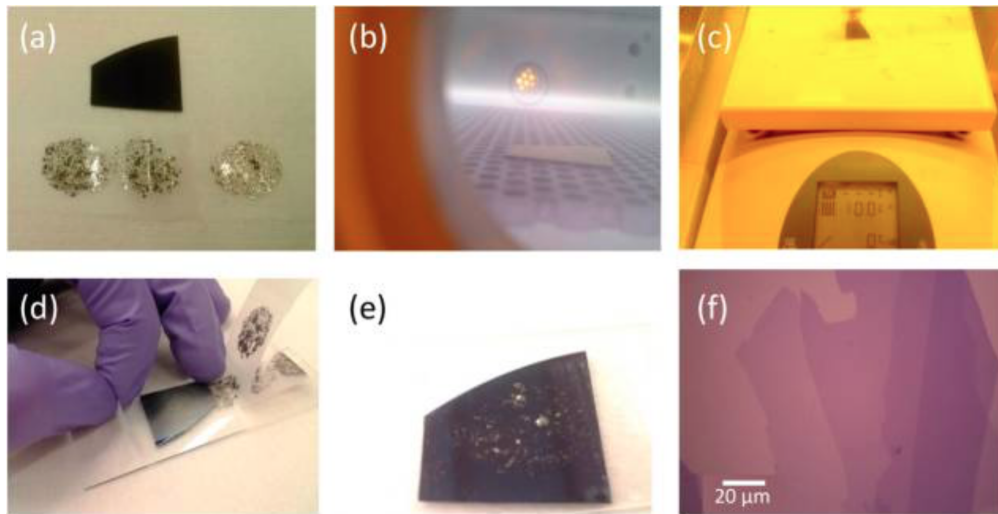


Figure 2.3: Illustration of a exfoliation process. (a) Optical image of the SiO_2/Si substrate and adhesive tape with graphite flakes. (b) Oxygen plasma cleaning of the SiO_2/Si substrate. (c) Heating of the SiO_2/Si -adhesive tape sandwich. (d) Peeling of the tape. (e) Optical image of the substrate after graphene exfoliation. (f) Microscope image of one of the graphene flakes on the substrate, lighter shades of purple indicate fewer layers of graphene.[20]

but in terms of quality, depending on the producer, your results may vary. Furthermore, presently there are no standardised quality criteria for CVD graphene, which makes it difficult to compare different types. At this moment, copper-based CVD is the most popular production method for deposition synthesis[32].

2.2.3 Reduction of graphite oxide

Another synthesis method that is often used is the reduction of graphite oxide. This method involves the oxidation of graphite to graphite oxide using oxidising agents. The graphite, when oxidised, undergoes an increase of both the interlayer separation as well as the material hydrophilicity, making it dispersible in water. Using sonication, graphite oxide can now be exfoliated, producing single to few-layer graphene, or graphene oxide[43]. During this process the flakes are functionalised with oxygen groups, causing differences in material properties from pristine graphene. The oxygen containing groups that are introduced by these chemical processes can provide anchoring groups to enzymes and other specific species for sensing applications. Up until now, this has been the approach to produce electrochemical sensors based on graphene. However, these chemical processes critically reduce the electrical conductivity. As the latter effect defeats the purpose of the goal of this project, graphite oxide was not considered in this thesis[10] and an alternative approach is investigated here.

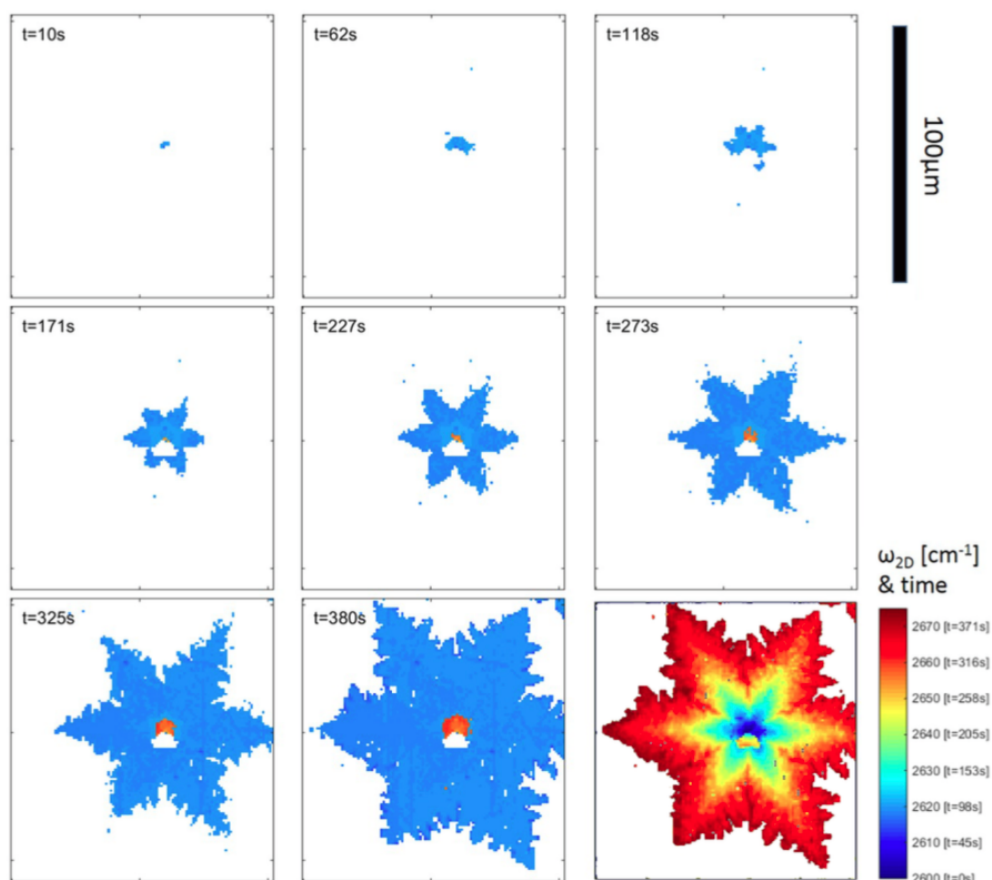


Figure 2.4: Visualisation of the growth of a CVD graphene grain. Two isotopes of carbon are alternately used in the precursor gas that are distinguishable through Raman spectroscopy. Bottom-right square summarises the growth process and shows the Raman shift and associated time[63]

2.2.4 Intermediate conclusion

In terms of quality, ME graphene is the best option for investigation of electrochemical characterisation when strained. If one would be able to measure the basal plane of a flake of ME graphene the direct influence of strain on the electroactivity can be observed. However, ME flakes are small ($\sim 10\ \mu\text{m}$ to $100\ \mu\text{m}$) and thus difficult to handle. CVD graphene can be synthesised in larger dimensions, which makes it easier to use but quality is lost due to grain boundaries which can have mechanical and chemical implications. Graphene oxide is relatively easy to functionalise but loses the properties that are trying to be exploited in this research.

2.3 Strained graphene

Two of the plentiful remarkable properties of monolayer graphene are its elasticity and strength: it has a Young's modulus of 1 TPa and an intrinsic strength of $\sigma_{int} = 130$ GPa[24]. In comparison, for A36 steel, a commonly used steel alloy, these values are 200 GPa and 330 MPa respectively, while being 7.8 times heavier[31]. One could argue that this extremely high mechanical strength makes it impossible to strain but it is important to remember that this strength has a unit of Pa, or Nm^{-2} . Due to the extremely low thickness of graphene (3.7 Å or 0.37 nm) the practical difficulties are more concerned with clamping than force exertion itself. On an atomic level, high amounts of elastic strain can change the material properties of graphene, which is what scientists have been trying to do and exploit for various goals.

It has been proposed to use strain to introduce a band gap in graphene, so-called *band engineering*, for electronic and optoelectronic applications[44]. However, tight-binding models and *ab initio* calculations give varying results, some claiming there is no band gap opening below 10% strain[50], while others have come up with a minimum required strain of at least 20%[12]. A band gap opening could make graphene a contender for the next generation of integrated circuits, which is why this is the direction most of the strained graphene research is headed towards. However, because of the high strain required (unattained up until now), band gap engineering will not be discussed in this thesis. Surface adsorption however, could be stimulated by strain, even at low levels, which is what will be examined in this section.

Presented here is a theoretical background of strain engineering of graphene, followed by an overview of the current methods to strain graphene relevant to the scope of this thesis.

2.3.1 Theory

In a relaxed state, the electrons of carbon atoms in a graphene lattice not used in covalent bonds are located above and below the hexagonal plane. When looking at the reciprocal lattice one can identify the first Brillouin zone, which has a hexagonal shape, as seen in Figure 2.5. The electronic dispersion in the honeycomb lattice has a particular shape (Figure 2.6) such that on the corners of the Brillouin zone (K and K' in Figure 2.5) the bonding and anti-bonding energy levels π and π^* 'meet' at the Fermi Level in the form of two cones: the Dirac cones. Where there is a small gap between those levels in conducting materials and a large gap in insulators, in graphene there is no gap at all. This allows for the electrons to hop to their nearest neighbour, resulting in ballistic transport on the submicrometer scale, even at room temperature[41], while chemical activity is minimised to maximise the bond order for the available number of valence electrons of carbon[1].

However, when graphene is strained, the interatomic distance is increased, shifting the

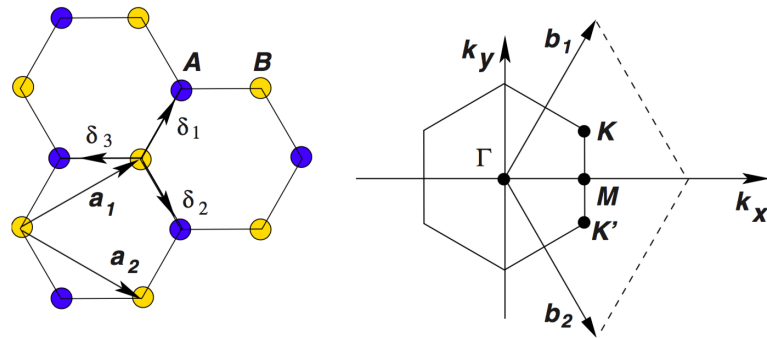


Figure 2.5: Left: schematic of carbon atoms in a graphene lattice. Right: the first Brillouin zone of a carbon atom in a graphene lattice.[37]

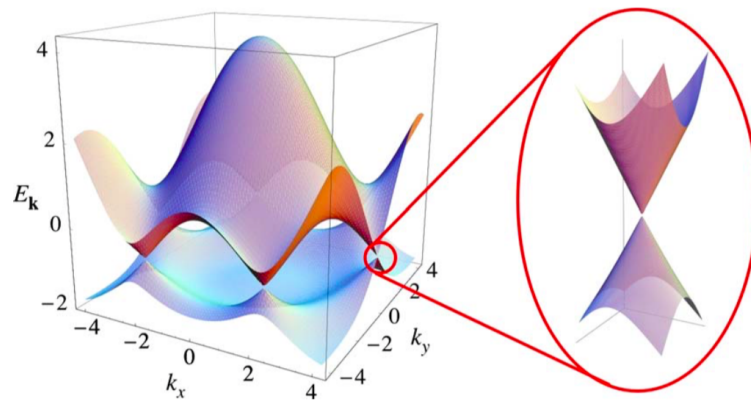


Figure 2.6: Schematic showing the energy spectrum of the π bonds. The right image shows the energy bands close to a Dirac point up close[37].

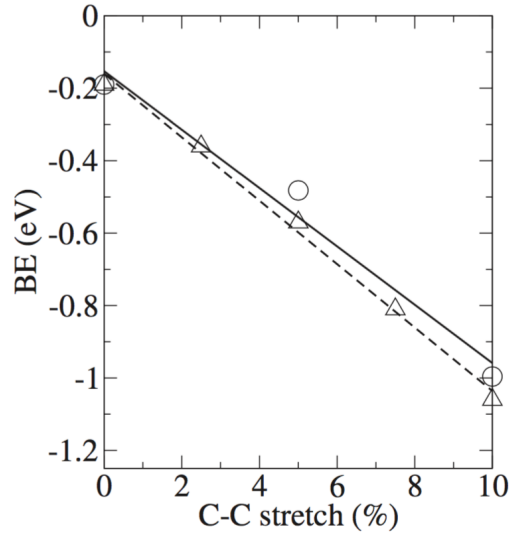


Figure 2.7: Results of ab initio calculations of the binding energy (eV) of H on graphene versus the C-C stretch (%) using two different modelling techniques[1]

Dirac cones away from the K and K' points (Figure 2.5), weakening the electron hoppings while extending the π orbital. When this happens, its configuration is changed from a sp^2 to a $sp^2 - sp^3$ like state and with it comes simultaneous loss of electronic conjugation[22]. The electron now becomes more localised around its atom and becomes available for a chemical reaction. Shift of the K and K' points can only happen when the graphene is strained uniaxially, as biaxial strain would only change the relative positions of the Dirac cones[14], while keeping the same hexagonal shape. This is why only uniaxial strain is considered in this research. This also disqualifies strain caused by nanoindentation. Lastly, the direction of strain with respect to the crystallographic edge directions of the graphene (zigzag and armchair) has different consequences for the electronic dispersion. When dealing with ME graphene, this has to be taken into account.

For a long time people have been searching for a new storage method for hydrogen with respect to for energy storage. Graphene has been one of the candidates, becoming *graphane* after taking up hydrogen, which is why a lot of research has been done on this type of covalent binding. *Ab initio* calculations have shown this phenomenon[1] and experiments done on carbon nanotubes (CNT's) confirm this theory. In Figure 2.7 it can be seen that strain linearly influences the binding energy of a H atom on the graphene lattice. Essentially, this means that it becomes easier for the hydrogen atom to covalently bind to the graphene when it is strained.

The amount of strain required for other molecules or atoms is not known and requires separate research for each functional group, this falls outside of the scope of this research.

Ruffieux et al.[51], have shown that the energy barrier for bond formation decreases

with local curvature, giving way for preferential atomic hydrogen adsorption. Wang et al.[62] extended this property to graphene and demonstrated (theoretically) how a compression-induced rippling could promote periodical hydrogen adsorption for band-gap control. Self-assembly of other species such as F, Cl, and O has been said to be catalysed by mechanical strain[54] but have not been modelled or experimentally tested, presumably due to the extremely high computational costs of computational (quantum) chemistry and practical difficulties respectively.

Bisset et al. has used a flexible substrate to strain CVD graphene, while being in contact with different aryl diazonium molecules in solution and measured the (self-)adsorption at different time instants[6]. Not only was the rate of activity increased up to 10 times with strain, it also acted as a catalyst for reactions that normally would not occur. They report that the strain transfer between the polymer substrate and the graphene is not ideal; strain is lost due to inefficient interfacial transfer mechanisms such as slippage and locally the strain can be 10-100 times larger than the applied strain. A maximum of 0.2% to 0.3% is reported as strain induced by polydimethylsiloxane (PDMS)[7]. Also, strain is not distributed homogeneously across the surface, which makes it difficult to determine the ‘real’ strain exerted on the graphene. Normally, this can be measured by looking at the Raman 2D peak shift (see Subsection 4.3.1). However, Bisset et al. use a form of functionalisation which causes p-type doping, which causes an upshift of the G and 2D peaks, clouding the strain/peak position relation. Furthermore, they observe that their method of straining does not induce damage in the graphene lattice. Lastly, an advantage of this approach for the purpose of this research is that the substrate is non-conductive, making it easier to design an electrochemical half-cell around it.

High amounts of strain were reported by Pérez Garza et al., who reported extreme strain on ME graphene (>10%) using a tensile microelectromechanical system (MEMS) depicted in Figure 2.8[46], which was readily available for this project. However, doubts have been expressed about the amount of strain measured by multiple researchers[47][59].

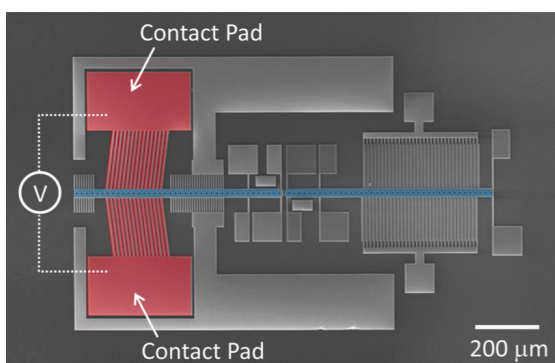


Figure 2.8: Tensile MEMS device, reportedly able to apply high strains (>10%) on graphene[46]

2.3.2 Intermediate conclusion

Although there has been much research regarding the use of strain in band gap engineering of graphene (without much result due to the extremely high strain required), tuning the chemical reactivity of graphene, which requires less strain, has been limited to applications in hydrogen adsorption with a few exceptions[7][6]. In order to change the chemical properties of graphene for surface functionalisation uniaxial strain has to be applied. Proven ways to uniaxially strain graphene involve the use of a tensile MEMS or a flexible substrate, the former being able to attain high strains (>10%), the latter significantly lower (0.2% to 0.3%), but easier in execution.

2.4 Electrochemistry of graphene

This section studies the electrochemistry of graphene and a comparable carbon allotrope. As this thesis is written for a Masters' thesis in Mechanical Engineering, there is a brief, general introduction to electrochemistry to be found in Appendix A.

Graphene was only isolated by Novosolev and Geim in 2004[39] and its recent isolation, in combination with handling difficulties, have limited the amount of electrochemical research done on this novel material. Other allotropes of carbon, however, have been common electrode materials used in electrochemical studies and are known for their *low cost, broad potential window, low background current, rich surface chemistry and comparative chemical inertness*[10]. In the past, glassy carbon was used as an electrode material but recently, Highly Orientated Pyrolytic Graphite (HOPG) has shown better electrochemical performance because of its well-defined structure, which has similarities to graphene. Overall, there have been only few reports of electrochemistry on monolayer graphene which is why this chapter is divided into three parts, namely the electrochemistry of HOPG, of mechanically exfoliated (ME) graphene and that of chemical vapour deposition graphene.

A few redox couples are mentioned in this chapter, sometimes by their chemical formula, sometimes by name. To prevent confusion, the mostly used couples are:

Name	Chemical formula
Ferri-Ferrocyanide	$\text{Fe}(\text{CN})_6^{4-/3-}$
Hexaamineruthenium	$\text{Ru}(\text{NH}_3)_6^{3+/2+}$
Ferrocenemethanol	FcMeOH

Table 2.1

2.4.1 HOPG

The isolation of graphene and research in carbon nanotubes (CNTs) have led to a huge increase of interest in HOPG, which is a form of synthetic graphite characterised by well aligned graphite crystallites. This newly sparked interest has also increased the research

done on the electroactivity of HOPG, from which new information has arisen.

Density of states and electron transfer As shall be seen with graphene, a distinction has to be made between the basal plane and the edge plane of HOPG, also when talking about electrochemistry. The basal plane can be compared to that of graphene (though with many underlying layers) and the edge plane, perpendicular to the basal plane, spans over multiple graphitic layers and can be seen as amorphous carbon. For a long time, the general consensus was that the basal plane of HOPG had extremely poor electrode kinetics, compared to its edge plane for multiple redox couples[9][21]. Some even claimed that the basal surface had no electroactivity[2][13]. This phenomenon was explained by relating the electronic density of states (DOS) to the electron transfer (ET). The DOS of a wave-like particle in a quantum mechanical system represent the number of states available at each energy level per unit volume. When talking about the electrode-electrolyte interface, it was believed that the electrons in the electrode material should have states with energies within the range of the donor or acceptor levels of the redox couple for a reaction to occur. A higher DOS of the electrode corresponds to a fast electron transfer in combination with a matching electrolyte. Incidentally, carbon atoms show extremes of DOS, with diamond on the low end of the spectrum, having a large energy gap and no states, and disordered graphitic materials, having a relatively even DOS distribution[33].

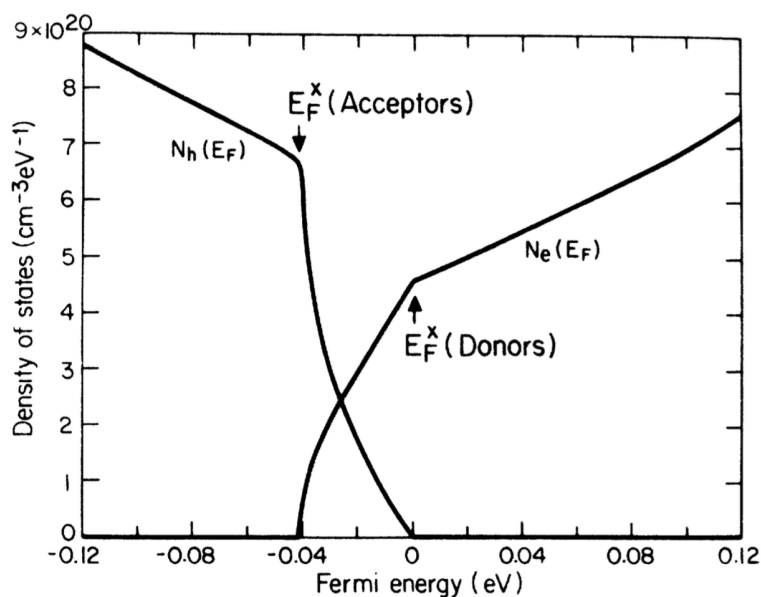


Figure 2.9: Calculated fermi-level dependence of the DOS $N_e(E_F)$ and $N_h(E_F)$ for electrons and holes showing a low DOS at the Fermi level[15]

On the basal plane of HOPG, the carbon atoms have three of their electrons in the

valence band in the sp^2 orbital, forming covalent bonds with three other carbon atoms. The fourth electron is delocalised and has several unique features, one of which is a low DOS at the Fermi level (Figure 2.9), about two orders of magnitude lower than those of metals[66], and thus low in electroactivity. In other words, edge or defect locations, where not all electrons are used for the so-called σ - and π -bonds (see Section 2.1), are the locations where most of the electron transfer (i.e., electroactivity) is possible. At these locations dangling bonds are present, which have a significantly higher DOS.

According to this theory, the basal plane should be very low in activity and whenever researchers measured higher ET than expected, it was attributed to the inclusion of edge and/or defect locations[2][13]. This was unavoidable because of their macroscopic cyclic voltammetry measurements, typically on areas >0.1 cm[23]. However, recent techniques have been able to do electrochemical imaging at higher resolutions, giving more accurate insight into the electrochemical behaviour of the basal- and the edge plane. Lai et al. were able to do measurements on areas with a diameter of 22 nm to 320 nm using scanning electrochemical cell microscopy (SECCM) and reported ET rate constants of >1 cm s^{-1} for the $\text{Fe}(\text{CN})_6^{4-/3-}$ couple as opposed to 10^{-5} cm s^{-1} to 10^{-9} cm s^{-1} in previous researches. Furthermore, voltammograms obtained with the two most studied redox couples, $\text{Fe}(\text{CN})_6^{4-/3-}$ and $\text{Ru}(\text{NH}_3)_6^{3+/2+}$ showed almost-reversible reactions. Furthermore, a time-dependency is noted; after exposure to air the surface is passivated, decreasing electroactivity in a matter of hours. Later that year (2012), Patel et al. were also able to measure ‘essentially’ reversible voltammetries using the same SECCM technique and observe the same passivation as noted above[42]. A warning is given regarding the use of the ferri-ferrocyanide redox couple: blocking and changes in surface conductivity is observed which can be avoided by using the $\text{Ru}(\text{NH}_3)_6^{3+/2+}$ couple. With the same electrolyte, Zhang et al. report a lower limit of the ET rate of 0.61 cm s^{-1} , comparable to that of metal electrodes and even question the direct relationship between the DOS at the Fermi level and electrode kinetics for outer-sphere redox couples (see Subsection 3.2.1).

2.4.2 Mechanically exfoliated graphene

A crucial point in determining the electroactivity of ME graphene is the electrical wiring to the graphene, which should be isolated from the electrolyte. Because of the maximum size of ME graphene as of now, it requires an extremely precise electrochemical setup. This is unfortunate, because ME graphene presently still yields the highest quality of graphene, e.i. single crystallites and few defects. Like with HOPG, the chemical reactivity of the edge and defect sites are expected to be different than that of the basal plane. Differentiation of the electroactivity between these two regions requires a certain contact area, which makes the experimental setups extra difficult: a second crucial point. Because of these technical difficulties, only few experiments have been done that investigate the chemical reactivity of ME graphene. An overview of the research done is presented in this subsection.

Graphene is generally found to be electroactive, both on the basal as on the edge plane. One could expect that the basal plane of graphene resembles that of HOPG in electroactivity, and until the recent reconsideration regarding HOPG (Subsection 2.4.1) its activity was expected to be negligible. However, Li et al.[26] did measurements on graphene and on HOPG and measured a k^0 value of FcMeOH that was two orders of magnitude larger on graphene than on HOPG (0.5 cm s^{-1} vs 0.007 cm s^{-1} respectively). They attributed their results to the micro-corrugations present in graphene which cause localised areas of strain; in the case of HOPG the presence of an underlying carbon layer prevents wrinkling. This causes a change in the electron density of the carbon atom in favour of the ET: a good sign for the hypothesis of this project. Defects in the lattice are not considered as cause for its high reactivity as Raman spectroscopy detected none. This was confirmed by Valota et al., who deliberately damaged pristine graphene and saw no change of the voltammetric response curves[58].

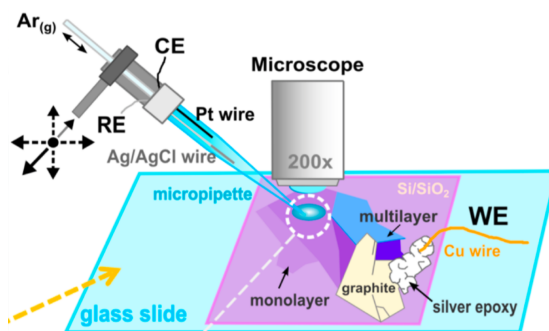


Figure 2.10: Schematic of experimental setup used by Velicky et al. [60]

On a single flake of graphene different values of electron transfer rate can be found. This variation is shown in particular by the extensive work done by Velicky et al.[60], who found ET variation of 12-31% on pristine mono-layer flakes with different redox couples, using a micropipette setup (Figure 2.10). $\text{Fe}(\text{CN})_6^{3-/4-}$ and $\text{Ru}(\text{NH}_3)_6^{3+/2+}$ gave the most variation, whereas $\text{IrCl}_6^{2-/3-}$ gave the most consistent results. Two possible sources for these variations are the aforementioned spacial corrugations and they add temporal surface contaminations as a cause, conclusions also made by other researchers[56].

Contamination of the surface naturally occurs when it is exposed to an ambient environment[58]. Oxygen, water or other chemicals present in the air can lead to a chemical modification of the graphene surface[60]. Contamination, leading to surface poisoning and passivation should thus be considered because it affects the electrochemical performance, with $\text{Ru}(\text{NH}_3)_6^{3+/2+}$ being especially sensitive to these effects, according to Velicky et al.[60]

2.4.3 CVD graphene

What is gained in ease of handling is lost in accuracy when doing electrochemical experiments with CVD graphene. As said before, the edge locations of graphene crystallites are different in reactivity than the basal plane because of lattice imperfections. Due to the production method, edge locations are intrinsically present in CVD graphene, though the grain sizes depend on the experimental settings.

Some researchers were able to compare ME and CVD graphene; Li et al. used FcMeOH as a redox couple on CVD graphene and saw ET rates that were one order of magnitude smaller than that of ME graphene (0.042 cm s^{-1} vs 0.5 cm s^{-1})[26], which they relate to the lower electron mobility of CVD graphene. Unfortunately, further explanation of this claim are not given.

Güell et al. did SECCM on graphene of various layers and observed irreversible reactions on monolayer CVD graphene with $[\text{FcTMA}^{+/2+}]$, increasing the amount of layers improved reversibility and the ET transfer rate constants k_0 (0.06 cm s^{-1} for monolayer vs 0.13 cm s^{-1} for seven layers). Furthermore, they report no increase of EC activity along the edges of the flakes or at the boundaries between flakes[19]. Yuan et al., however, reported that the edge-plane was at least 2 orders of magnitude stronger than the basal-plane in terms of current density with the ferri-ferrocyanide couple. They were able to mask part of the CVD graphene electrode with epoxy resin to isolate the basal plane; vertical cutting exposed the edge-plane[65].

Tan et al. investigated the effects of mechanically and chemically induced defects in a CVD monolayer using scanning electrochemical microscopy (SECM) and observed very different electron transfer kinetics. Feedback currents at mechanically induced defect sites were an order of magnitude larger than those of bulk graphene ($2.6 \times 10^{-4} \text{ cm s}^{-1}$ vs $4.5 \times 10^{-5} \text{ cm s}^{-1}$ respectively)[55] and refer to the research done on HOPG mentioned in Subsection 2.4.1 by McCreery et al.

2.4.4 Intermediate conclusion

The field of graphene electrochemistry is in its initial stage, but electrochemical microscopy has progressed the field even giving new insight in the electroactivity of HOPG. The consensus used to be that it was only chemically active at edge and defect sites but new, small-scale techniques have shown activity on the basal plane too. ME graphene appears to be even more electroactive than HOPG: this is attributed to the intrinsic corrugations present in monolayer graphene causing local areas of strain. Some practical issues regarding graphene electrochemistry:

1. An issue with graphene electrochemistry is the maximum size of the electrical wiring, especially with ME graphene, which has limited the electrochemical characterisation of graphene.
2. Cyclic voltammetry is the technique of choice as electrochemical characterisation tool to study graphene.

Finally, some previous observations to keep in mind when doing the experiments:

1. There is uncertainty regarding the difference of electroactivity between the grain boundaries and the basal plane of CVD graphene.
2. Defects are reported to have no effect on the electroactivity of ME graphene. Surface contamination, however, is an issue.

2.5 Conclusion

Regarding the strain of graphene, there are several techniques to attain different amounts of strain, of which a tensile MEMS device, available to the author of this document, attains the highest amount of strain ($>10\%$) on ME graphene. Furthermore, flexible substrates are able to strain CVD graphene but have their limitations in terms of maximum strain and inhomogeneous stress distribution. The eventual strain required is dependant on the species that will functionalise the graphene.

As opposed to band gap engineering and strain-induced hydrogen storage, the field of strain engineering to chemically tune graphene is very immature, but highly promising nevertheless. The electroactivity of graphene, even on the basal plane has been observed as above expectations, attributed to the local corrugations introducing areas of strain, which in turn improve electroactivity. Furthermore, theoretically this has been confirmed for the covalent bonding of atomic Hydrogen. If this could be expanded to a more general statement in which a certain amount of strain allows for specific species to attach, a whole new world of graphene strain engineering opens up. Further research could be directed towards the generation of strain for specific functional groups for virtually infinite applications.

As there are no reports on the use of strain to improve electrochemically induced covalent bonding on the surface of graphene, it is clear that an investigation will be appreciated. However, because of the novelty of this field of research, comparison of quantitative data with literature will be difficult and experimentally speaking, creativity is required.

3 Design of an experimental setup for electrochemistry in a drop

3.1 Introduction

The first experimental part of this project consists of the design and characterisation of an electrochemical setup that is able to use graphene as a working electrode and measure a current flow through the electrode-electrolyte interface when a potential is applied. The size of the available graphene sample limits the size of the experiment such that in this case, the electrolyte has to be in the form of a droplet. The design was done in two steps; a setup for a graphite flake and one for a graphene monolayer. The decision is made to test the system with cyclic voltammetry, a widely used electroanalytical tool to study electron transfer kinetics and electrode behaviour characterisation[52].

3.2 Cyclic voltammetry

The method chosen for the electrochemical characterisation in this thesis is cyclic voltammetry (CV), this section will explain the basic mechanisms behind CV and its function.

In CV, an electrode is put in contact with a liquid containing the ions of a redox couple (the electrolyte); current flow between these two is measured caused by the electric potential applied. The potential is increased (or decreased) at a certain rate until a maximum (or minimum), after which it is reversed. The return at the initial potential value marks a complete CV cycle. A typical CV setup is shown in Figure 3.1a.

One can identify several components in Figure 3.1a:

- Working electrode (WE): consists of the material that is being researched.
- Reference electrode (RE): an electrode that is kept at a constant potential. The reaction-driving potential (\mathbf{V}) is applied between the RE and the WE but no current flows to or from the RE.
- Counter electrode (CE): acts as a current source or drain, depending on the direction of the current. The current measured at \mathbf{A} is the output of the system.

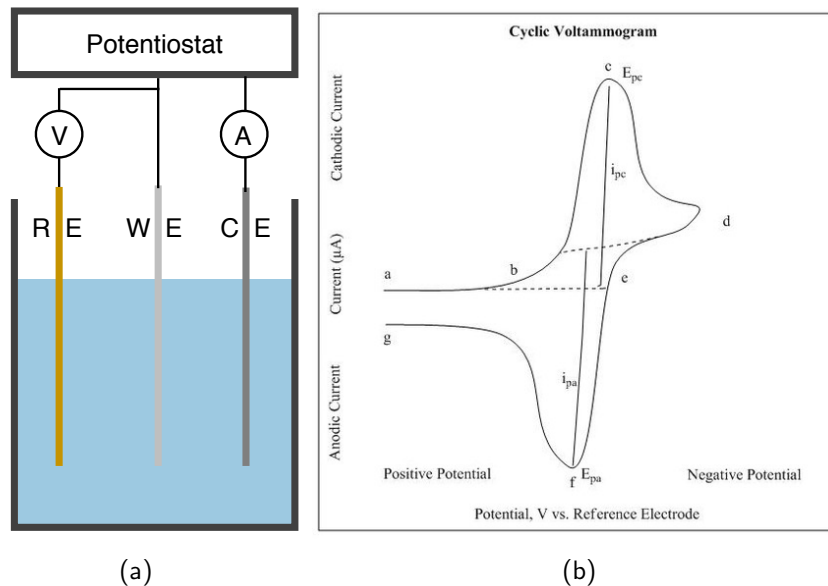


Figure 3.1: a) Schematic setup of a classic cyclic voltammetry setup. b) Typical result of a cyclic voltammetry experiment [5].

- Potentiostat: acts as an interface for the system, controls the voltage difference and current measurements and depending on the machine at hand, allows for complex, automated programs.

Next to the electrolyte, the liquid contains a supporting electrolyte that should not be electroactive in the range of the potentials used and is meant to increase the conductance of the system.

Figure 3.1b shows a typical cycle of a voltammogram, where one can identify a couple of different regions in the graph. From point a to d the voltage is decreased linearly from a high positive value to a high negative value. At point b the potential is sufficient to start the reduction of the cations in the vicinity of the WE. At point c it reaches a maximum with corresponding cathodic peak current (i_{pc}) and potential (E_{pc}), and after this point the zone surrounding the electrical double layer (EDL) has been depleted from cations. When further decreasing the potential the current flow is dominated by the diffusion of ions (mass transport) through the liquid (non-faradaic current), which is usually a slower process than the current caused by the reactions of the electrolyte (faradaic current). The potential is reversed at d and the current follows a similar, opposite path, where i_{pa} and E_{pa} are the anodic peak current and potential respectively.

When the reaction is fast enough to maintain the concentrations of the redox couple in equilibrium with each other at the electrode surface after a cycle, the process is said to be *reversible*, which can be checked with the following criteria:

1. The peak potential separation, ΔE_p is close to $58 \text{ mV}/n$ (at 25°C) where n is the amount of electrons transferred per molecule.
2. The peak current ratio i_{pa}/i_{pc} is one (1) at all scan rates.
3. The relation between the peak current (i_p) and the square root of the scan rate (v) is linear.
4. The peak potential of does not change when changing the scan rate.

Slight deviation or partial compliance to these criteria makes the system irreversible or quasi-reversible.

The Nernst equation gives the equilibrium ratio at a certain potential at the electrode surface of a reversible system:

$$E = E^{0r} - \frac{RT}{nF} \ln \left(\frac{[R]}{[O]} \right)_{x=0}, \quad (3.2.1)$$

where E is the applied potential; E^{0r} is the formal reduction potential; R is the universal gas constant; T is the temperature and $[R]$ and $[O]$ the concentrations of the reduced form and oxidised form respectively.

The relation between the peak current and the scan rate of a reversible system is

$$i_p = (2.69 \times 10^5) n^{3/2} A D_0^{1/2} v^{1/2} C_0^*, \quad (3.2.2)$$

where A is the electrode surface area, D_0 the diffusion coefficient of the oxidised form and C_0^* the bulk concentration[29].

3.2.1 Electrolytes, electrodes

Before starting with the cyclic voltammetry (CV) measurements the electrolytes and electrode material should be chosen appropriately. In order to maximise comparability between the different CV experiments, the same electrolytes and electrode material are used for all experiments. As the main goal is to characterise monolayer graphene, the electrolyte is chosen for this condition and used for the other experiments. An overview of the electrolytes and electrodes used in previous studies on graphene and HOPG can be found in Table 3.1.

According to Velicky et al., $\text{Ru}(\text{NH}_3)_6^{3+}$ causes slightly more variations in the response than $\text{Fe}(\text{CN})_6^{4-}$, while IrCl_6^{2-} is the least sensitive to these variations. In order to study these variations, $\text{Fe}(\text{CN})_6^{4-}$ and $\text{Ru}(\text{NH}_3)_6^{3+}$ are used in this research. In terms of electrode material, platinum and silver are used most frequently except for Guell and Lai, who are using two Ag/AgCl quasi-reference counter electrodes (QRCE), often used in scanning electrochemical cell microscopy (SECCM).

Author	Type	Electrolyte	Supporting	CE, RE
Li	ME monolayer	5.2 mM FcMeOH	1 M KCl	Pt wire, Ag/AgCl
	CVD monolayer	5.2 mM FcMeOH	0.1 M KCl	
Valota	ME Monolayer	1 mM $\text{Fe}(\text{CN})_6^{3-}$	3 M KCl	Pt wire, Ag/AgCl
	ME Multilayer	1 mM $\text{Fe}(\text{CN})_6^{3-}$	1 M KCl	
Guell	CVD mono- & multilayer SECCM	2 mM FcTMA ¹⁺	30 mM KCl	QCRE Ag/AgCl
Tan	CVD monolayer SECM	1 mM FcMeOH	0.1 M KCl	Pt wire, Ag/AgCl
		2 mM $\text{Fe}(\text{CN})_6^{3-}$	0.2 M PBS	
Yuan	CVD monolayer	5 mM $\text{Fe}(\text{CN})_6^{3-}$	0.1 M KCl	Pt foil, SCE
	CVD monolayer	0.1 M PBS	0.1 M KCl	
Toth	ME mono- & multilayer SECCM	5 mM IrCl_6	6 M LiCl	Pt wire, Ag/AgCl
Velicky	Monolayer	3 mM $\text{Fe}(\text{CN})_6^{3-}$	6 M LiCl	Pt wire, Ag/AgCl
		3 mM $\text{Ru}(\text{NH}_3)_3^{3+}$	6 M LiCl	
		3 mM IrCl_6^{2-}	6 M LiCl	

Table 3.1: Overview of research done on the electroactivity of graphene in order of publication

3.3 Graphite CV

As a first preparatory experiment, cyclic voltammetry is done on a graphite sample to get acquainted with cyclic voltammetry and to build a preliminary test setup. Graphite shares various material properties with graphene and is thus used as a first step in creating a graphene based electrochemical setup.

3.3.1 Methods and materials

The graphite is procured from a block of Highly Oriented Pyrolytic Graphite (HOPG), which, in essence, are stacked layers of graphene. The flake size that can be removed from the block is in the millimetre range and can thus be handled relatively easy. A set-up is built with the following requirements:

1. Redox reactions are allowed to happen between the graphite-electrolyte interface
2. The subsequent current flow can be measured
3. The set-up can be used for future experiments with graphene

A schematic of the setup can be found in Figure 3.2a, Figure 3.2b shows the view through the microscope camera to monitor the droplet size and electrode location. Figure C.1 in Appendix C shows the final setup.

In the setup built, a flake of graphite is exfoliated from the block of HOPG and is placed on a SiO_2/Si substrate. A drop of water containing the electrolyte and supporting electrolyte is deposited on the graphite sample while ensuring it doesn't cover the whole flake, leaving room for the CE connection. A platinum wire is pressed on the flake outside of the droplet and two electrodes are immersed in the droplet; a hand-made Ag/AgCl reference electrode (RE) and a Platinum wire counter electrode (CE). A description

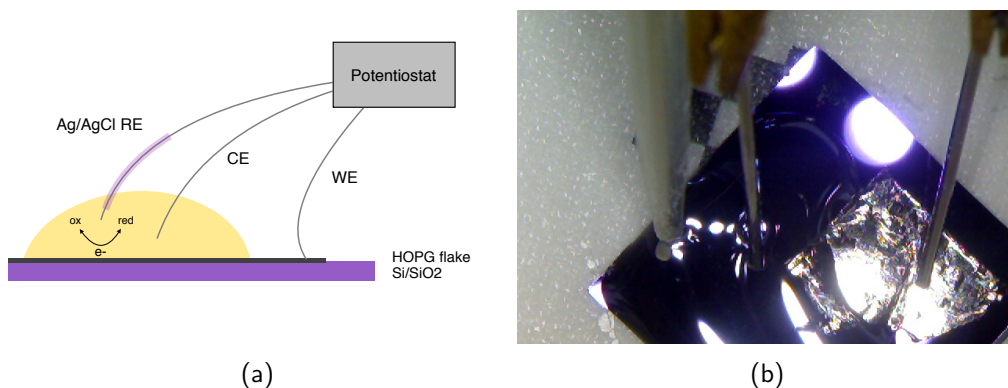


Figure 3.2: a) Schematic setup of the graphite CV setup. b) Droplet monitoring through microscope camera. (c) Overview of the graphite CV setup

of the production of the Ag/AgCl reference electrode can be found in Appendix B. The electrode wires are connected to the appropriate inputs and outputs of a Metrohm Autolab M101 potentiostat via three Suss MicroTec PH100 probeheads. The probeheads are used to precisely position the electrodes. A microscope camera is used to monitor the electrode positions and droplet size, as seen in Figure 3.2a.

3.3.2 Results and discussion

The current response of the graphite CV can be seen in Figure 3.3a. Linearly increased potential levels are applied at a rate of 100 mV/s and the subsequent current flow through the graphite-electrolyte interface is recorded.

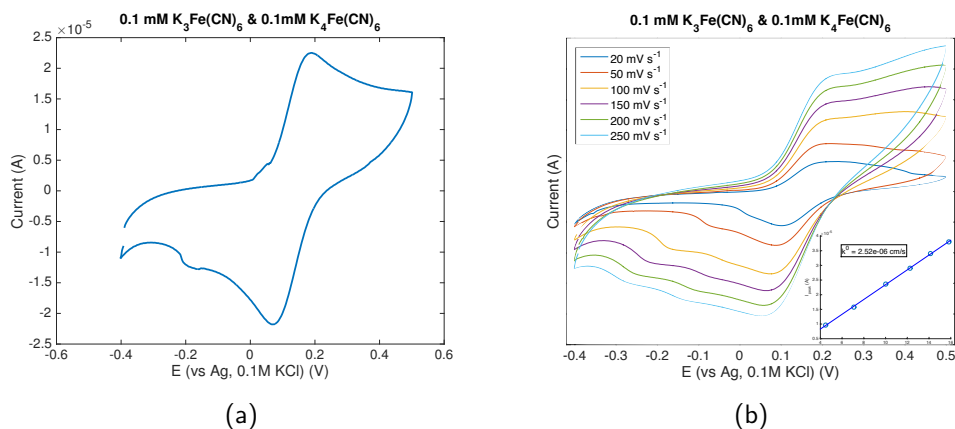
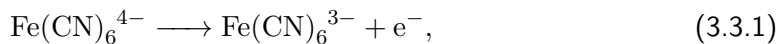


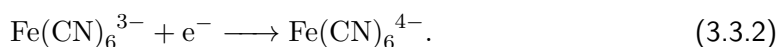
Figure 3.3: a) Cyclic voltammogram of a flake of HOPG. b) Magnitude of the oxidation peaks against the square root of the scan rate.

Figure 3.3a shows a typical cycle of a ferri/ferrocyanide voltammogram after stability sets in after a few cycles. An increasing potential is applied between the WE and RE at

a certain voltage rate and current starts to flow between the WE and the CE, initially non-faradaic. After the potential reaches a certain level it induces the following oxidation reaction:



which reaches a peak at a potential of 0.19 V. At this point, most of the anions in the electrical double layer (EDL) have been oxidised and when further increasing the potential the current flow becomes dependant on the diffusion of ions through the liquid. When the potential has reached 0.5 V, the voltage rate is reversed and -even though initially it is sufficiently positive for the oxidation of Equation 3.3.1- at some point the cations are oxidised according to Equation 3.3.2:



At 0.07 V the reaction rate reaches a maximum after which most of the cations in the EDL have been reduced and again, the current becomes non-faradaic.

Figure 3.3b shows the linear relation between the magnitude of the oxidation peak and the square root of the scan rate. The peak separation ΔE_p is 120 mV which makes the reaction quasi-reversible. A possible explanation is unwanted reactions happening at the interface or with contaminants as a mild disturbance can be seen in the graph at around -0.2 V. Further research is not done as the setup has been proved to work.

3.4 Graphene CV

As a next step towards the end-goal, graphene was used as an electrode and subjected to potential sweeps in a relaxed state.

3.4.1 Methods and materials

A CVD-grown graphene monolayer (Graphenea, 4" Si/SiO₂ wafer) is chosen as the working electrode. The graphene source is chosen for its substrate, which has a shallow native oxide layer acting as an electrical insulator and being chemically stable. This way, mainly the electrochemical response of the graphene is measured without having to transfer it to another substrate. A Pt wire is connected to the graphene with electrically conductive silver paint (RS Components) that connects the graphene to a potentiostat. The chip is used with the setup shown in Section 3.3 and cyclic voltammetry is done to check the characteristics of the electrode. The microscope camera was moved to capture a sideview such that the contact angle of the solution can be monitored (Figure C.2 in Appendix C).

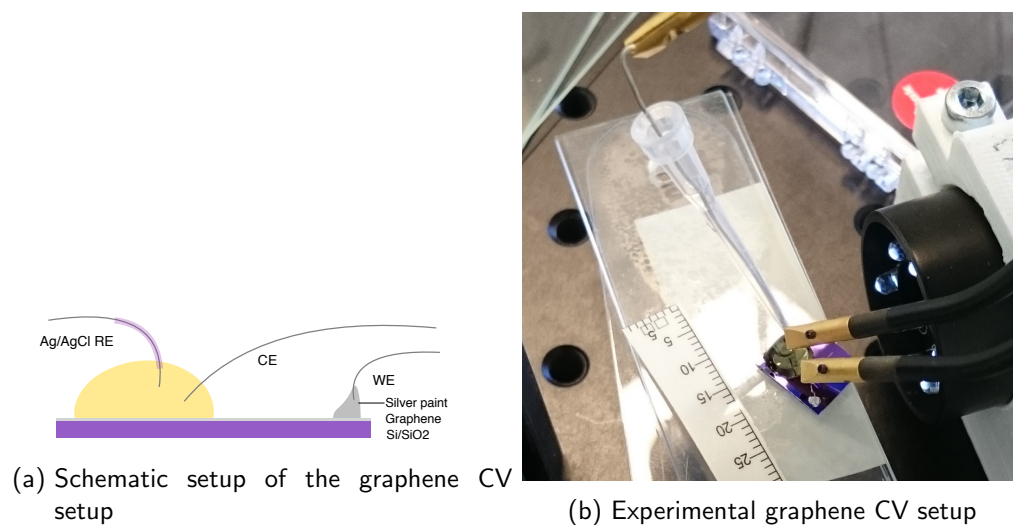


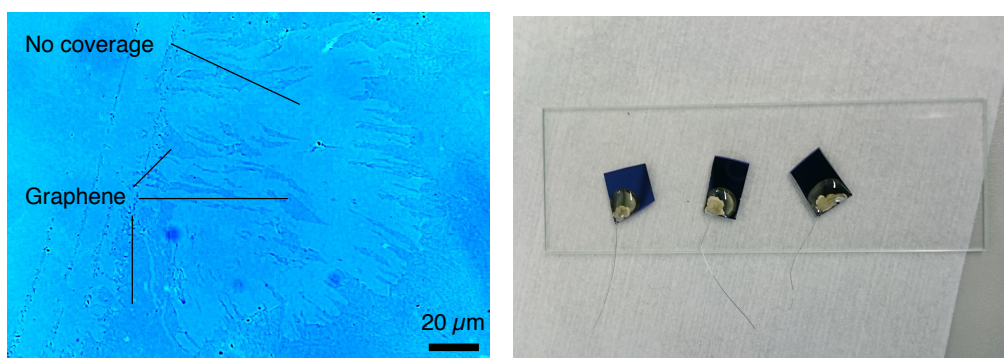
Figure 3.4

3.4.2 Results and discussion

Multiple chips were made using the method described in the previous section and subjected to CV scans. Supporting figures of the measurements can be found in Appendix D.

Two types of responses First of all it should be noted that the responses varied from chip to chip, which made it difficult to perform all the experiments that were initially planned. On approximately 10% of the chips a current response with visible peaks was measured, on others no peaks could be distinguished, showing only non-faradaic currents. The high variability of the chip responses was, after optical inspection of the chips, attributed to two causes. First of all, the poor coverage of the graphene on the substrate. As can be seen in Figure 3.5a, graphene does not fully cover the surface. For reactions to happen, an uninterrupted ‘path’ of graphene should be present from the Pt connection to the surface covered by the droplet. When it is not or only partially present, few or even no reactions can happen and no peaks can be observed. As this was not foreseen previously, the chips were made to be single-use, which meant that a lot of samples were needed and ‘good’ chips had to be thrown away. A simple augmentation, namely the securing of the silver paint connection with a two-component (insulating) epoxy, made the chips ready for multiple use (Figure 3.5b). Furthermore, the decision was made to use a different source of graphene for the next part of the research.

Secondly, it can be seen that currents were higher at measurements where no peaks were observed. At these measurements capacitive, non-faradaic behaviour could be observed (Appendix D). This means that a electrical connection from the WE to the CE must have been present. This rebuts the claim made earlier regarding the electrically insu-



(a) Microscope images of the Graphene (b) Three CVD graphene chips with 2-component epoxy securing the silver paint

Figure 3.5

lating role of the native oxide layer of the substrate. Possibly the substrate had defects that allowed the solution and the silver epoxy to come into contact with the underlying Si layer. Careful evaluation of the voltammograms has to be done, next to gentle handling of the substrate such that the current response of the silicon substrate does not overshadow the peaks of the graphene-ferri/ferrocyanide interface..

A stabilised potential cycle is shown in Figure 3.6. Oxidation and reduction peaks can be found at 0.19 V and 0.09 V respectively. Note: only part of the cycle is shown, containing the ferri-ferrocyanide peaks.

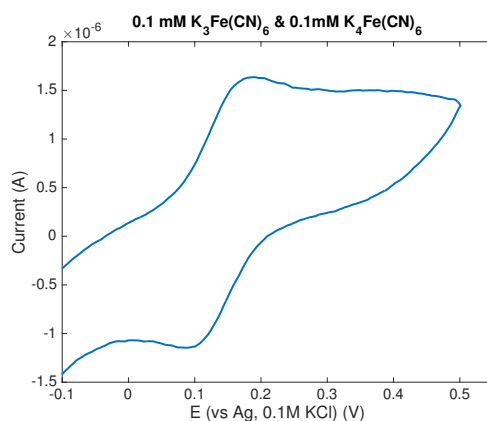


Figure 3.6: Cyclic voltammogram of a CVD-grown graphene monolayer

Due to the low yield of successful chips and limited availability of the Graphenea CVD graphene, the decision was made to skip the production of new chips which were supposed to measure the current response at varying scan rates. The results presented in this section prove the functioning of the system and as it will be used with graphene from a

different source, on a different substrate, the decision was made to start the production of the stretchable graphene electrode.

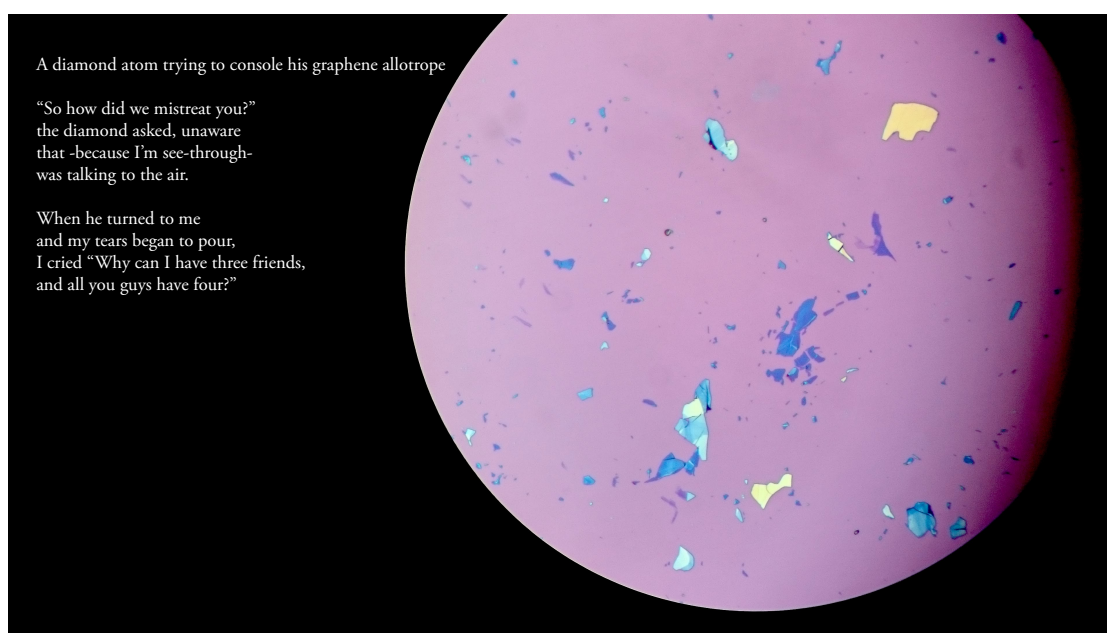
3.5 Summary and conclusion

An easy-to-build setup was designed and built that is able to connect an electrolyte in a droplet to a miniature electrode. The setup was tested with a flake of graphite and a monolayer of CVD graphene on a silicon substrate. A quasi-reversible reaction was measured between a graphite flake and the ferri-ferrocyanide redox couple.

Next, the setup was used which used commercially-bought CVD-grown graphene as electrode material. The yield of successful chips was approximately 10% which was attributed to the poor coverage of graphene on its Si/SiO₂ substrate and the electrical influence of the substrate.

Initially, the next planned step was the miniaturisation of the experiment described above such that the setup was able to use a flake of ME graphene (in the order of $\sim 10\ \mu\text{m}$) as electrode. However, because of time limitations, the decision was made to continue first with the production of the stretchable graphene electrode. The setup built is appropriate for graphene electrodes in the millimetre scale, limiting further research to CVD graphene as opposed to ME graphene. In this way, a measurement could be done on strained CVD graphene and if successful, a follow-up could be done with ME graphene. A plan has been written for this last experiment which can be found in Appendix E.

4 Design and production of a stretchable graphene electrode



4.1 Introduction

This chapter describes the design, production and characterisation of a stretchable graphene electrode, to be used in the electrochemical setup from Chapter 3. The goal is to apply controlled strain to a graphene sheet that is in contact with an electrolyte-containing droplet of water while having a separate electric connection. In this way it can be used as a working electrode in an electrochemical half-cell. Two different graphene sources are available: mechanically exfoliated (ME) graphene and chemical vapour deposition (CVD) graphene on a Cu substrate. Each is transferred to a Polydimethylsiloxane (PDMS) substrate using a different transfer method, both methods eventually allow for a substrate-induced strain, which strains the graphene due to interfacial stress transfer

between the PDMS and the graphene. After the transfer, strain characterisation is done to relate the strain applied to the PDMS to the strain measured in the graphene lattice.

4.2 Intermission: issues regarding uniaxial strain with a tensile MEMS

This project was started as one of the follow-ups of a PhD thesis at the same department, in which extreme strains were observed of graphene using a microelectromechanical system (MEMS). Initially, this strain approach was taken but half-way during the project the decision was made to abandon this approach and continue with strain exerted by a flexible substrate. A short motivation for this decision is reported in this section.

Pérez Garza et al. observed strains $>10\%$ on graphene using a tensile MEMS[46] in 2014. This MEMS was developed and made use of a thermally actuated shuttle, as shown in Figure 4.1. The thermal beams (in red) are heated by Joule heating after a voltage is applied on the contact pads, causing the shuttle to move. Multiple samples of varying layers of graphene were attached to this shuttle and to a load cell on the other side using epoxy. After applying a 12.5% strain on a three-layer sample the G-band showed a very small Raman shift and no splitting, the 2D-band remained almost static. Both bands did show a considerable decrease in intensity, namely 4.4% and 3.3% per percent strain for the G and 2D-band respectively. For a bilayer sample, a shift of -4.6 cm^{-1} was measured of the G-band and the 2D-band showed a shift of -58.9 cm^{-1} for a partially clamped layer and -372.4 cm^{-1} for a fully clamped layer subjected to 14% strain.

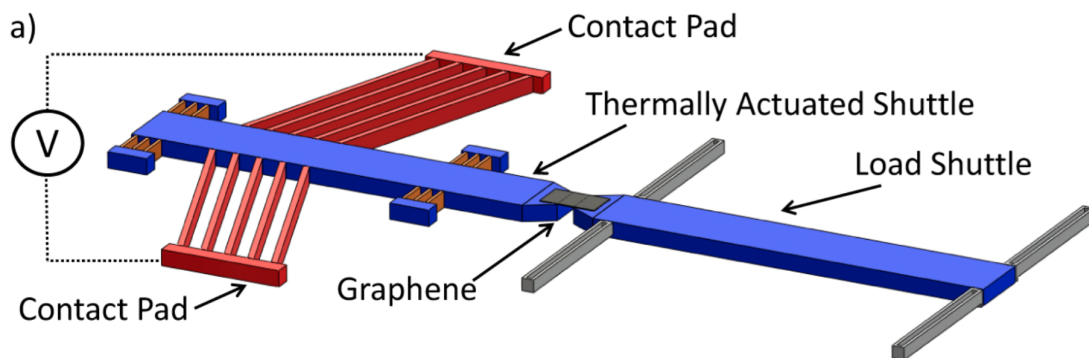


Figure 4.1: Schematic of a tensile MEMS developed to strain graphene[46]

In 2015, Polyzos et al. criticised aforementioned results, specifically the explanation of the absence of the expected peak shifts. The fact that the 2D peak shift was 3 times lower than expected and its origin unclear (it shifts after materialising at a certain applied strain setting instead of gradually shifting from the original position) gives rise to

doubts as to whether strain was applied fully or at all[47].

In 2016, van Omme, assisted by Pérez Garza, strained two multilayer ME graphene samples using the same type of MEMS and observed an maximum shift of -5% of the G-band and no trend of the 2D band at a strain of 12.5 cm^{-1} , comparable to Pérez Garza's results[59]. However, he attributes this shift to the temperature increase of the graphene and consider it highly questionable that the graphene was strained, expressing doubts regarding the results of Pérez Garza. Also, there were many practical difficulties regarding the transfer and thus an extremely low yield of successful chips to strain, which van Omme tried to circumvent by using large foils of CVD graphene. However, this was to no avail, as in the end no significant peak shifts were measured.

Thus, as the results achieved with the tensile MEMS were found to be controversial and low in terms of reproducibility, the decision was made to take an alternative approach, namely the use of a flexible substrate, as is shown below.

4.3 Materials and methods

This section gives a detailed description of the materials and methods used for the production of the stretchable electrode. First, a brief introduction into Raman spectroscopy is given, a well-known graphene characterisation method. Next, the transfer method used for each graphene type is shown, followed by a strain characterisation method for CVD graphene on Cu.

4.3.1 Raman spectroscopy of graphene

Raman spectroscopy is a measurement method that is based on the molecular vibrations of the electrons present in bonds. It is widely used in the scientific world as well as in industry for sample identification and characterisation. Also in graphene research Raman spectroscopy is one of the mostly used characterisation tools, being able to detect graphene, determine the amount of layers and defects while not doing any damage to it.

Introduction to Raman spectroscopy The underlying mechanism which is exploited by Raman spectroscopy is the temporary absorbance of photons in the form of energy. By firing monochromatic light at a sample at a certain frequency, its molecules can be excited to a higher (virtual) energy state. When a molecule returns to a lower state (after $\sim 10^{-14}$ s), it emits a photon corresponding to the energy difference between the excited state and the end state. There are various scenarios with respect to the excited state and the end state, as can be seen in Figure 4.2.

When the end state is equal to the initial state (elastic scattering), the molecule has undergone Rayleigh scattering, from which little information can be extracted. However, from (anti-)Stokes scattering, information characteristic to the material involved can be deduced. Its intensity is measured and can act as a 'fingerprint' of the material. The

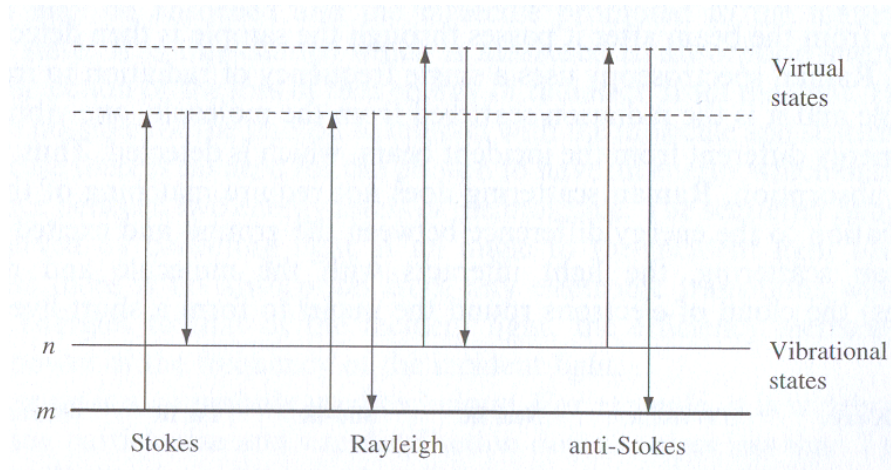


Figure 4.2: Energy states involved in Raman spectroscopy[17].

unit used in Raman spectroscopy is inverse length, corresponding to energy in cm^{-1} , or *wavenumbers*. Rayleigh scattering occurs far more often than Stokes scattering, thereby requiring a relatively long measurement to correctly determine the intensity relative to the other wavenumbers. The intensity is dependant on the measurement time which can be increased to reduce noise, which means that it is always represented with arbitrary units (a.u.)[57]. From the measurement a graph is made, from which the relative intensity of the peaks and their wavenumbers are used for the material characterisation.

Raman spectroscopy on graphene Raman is widely used for the detection and characterisation of graphene. Three peaks can be recognised when measuring graphene and with these three peaks are used to determine the number of layers, defects, strain and doping and other characteristics.

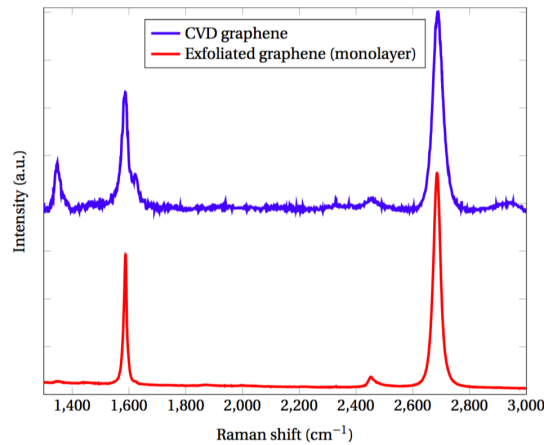


Figure 4.3: Typical Raman spectrum of graphene with blue light (514 nm)[59].

In Figure 4.3 the three typical bands of graphene can be identified when looking at the blue line:

- D band: the ‘defect’ or ‘disorder’ band, at $\sim 1350 \text{ cm}^{-1}$. Its intensity is proportional to the amount of defects in the graphene lattice. It is caused by the breathing modes of the sp^2 rings but only when it is next to a defect or plane edge.
- G band: a prominent band of all graphitic materials, at $\sim 1579 \text{ cm}^{-1}$. its position is unaffected by laser frequency but sensitive to doping and stain.
- 2D band: the second order of the D band, at $\sim 2692 \text{ cm}^{-1}$. but does not need a defect to be present. Like the G band, it is strong and often easily recognised.

Interpretation can give a lot of information about the graphene measured:

- The ratio between the intensity of the 2D band and the G band ($I_{2D/G}$ ratio) gives information about the amount of layers: monolayer, bilayer and trilayer have an $I_{2D/G}$ ratio of $\sim 2-3$, ~ 1 and $\sim .45$, respectively[45].
- Both the G and the 2D band are sensitive to strain; the G band splits into two bands moving in opposite direction, the 2D band redshifts.

Because the 2D band is the most prominent in the measurements in this report (mostly monolayer graphene), the strain will be derived from the 2D band peak shift, as is done in comparable strained graphene research[7]. Values for the shift-per-strain ratio vary from $-10 \text{ cm}^{-1}/\%$ to $-64 \text{ cm}^{-1}/\%$ [35][38].

All Raman spectra were acquired with a laser excitation energy of laser excitation energy of 2.41 eV, corresponding to a green laser with a wavelength of 514 nm and a spot size of 0.5 μm with a Horiba Labram HR Raman spectroscope.

Peak fit Peak fits were done using a least squares Lorentzian curve fit as seen in Figure 4.4. A normalised mean residual was calculated by dividing the mean residual by the peak height and was always kept under 1×10^{-6} .

4.3.2 Transfer

In the following paragraphs the protocols for the transfer of ME graphene and CVD graphene to a PDMS substrate (SYLGARD 184 silicone elastomer kit, Dow Corning) will be given.

ME graphene This method is based on the process described by Novoselov and Geim in 2004[39] with additional changes from Huang *et al.* in 2015[20] for an increased yield of flakes. Steps 6-8 were added to the protocol to produce a flexible substrate.

1. Adhesive tape is pressed against a highly oriented pyrolytic graphite (HOPG) crystal

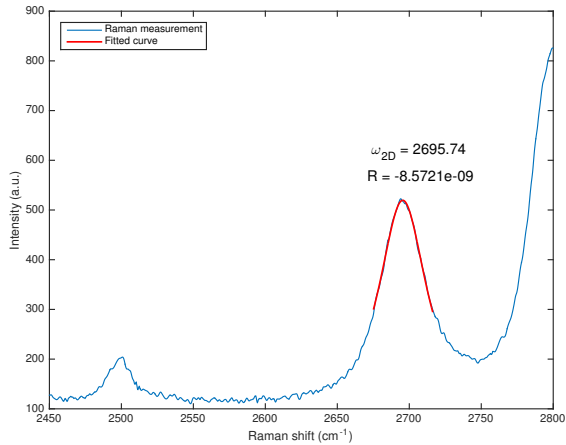


Figure 4.4: Lorentzian fit of the 2D curve of a measurement done on graphene on a PDMS substrate.

2. When the tape is peeled off, an indeterminate amount of the top layers of the HOPG adhere to the tape
3. The tape is pressed on a 285 nm SiO₂/Si substrate, which has had surface preparation by ultrasonically cleaning it in acetone, 2-propanol and deionised (DI) water, and completed by exposure to oxygen plasma to remove the last adsorbates.
4. The substrate with the tape attached is heated for 3 min at 100 °C on a hot plate
5. After the tape is removed, the flakes that are transferred to the substrate are studied and recorded with an optical microscope, as seen in the figure at the beginning of this chapter.
6. The SiO₂/Si substrate is glued to a petri dish and covered with liquid PDMS
7. After curing, the PDMS is peeled off and studied under a microscope to check the transfer
8. Raman spectroscopy is used to detect graphene and to determine the amount of layers

CVD graphene Graphene was acquired from Dr.ir. Vollebregt from the department of microelectronics at the Delft University of Technology. It was produced on a Si wafer, thermally oxidated to produce a 100 nm layer of SiO₂ on which a layer of 500 nm copper was deposited through magnetron sputtering. The gas mixture containing methane, argon and hydrogen was led along the copper surface at ~875 °C. Then the sample was transferred to a PDMS substrate as illustrated in Figure 4.5.

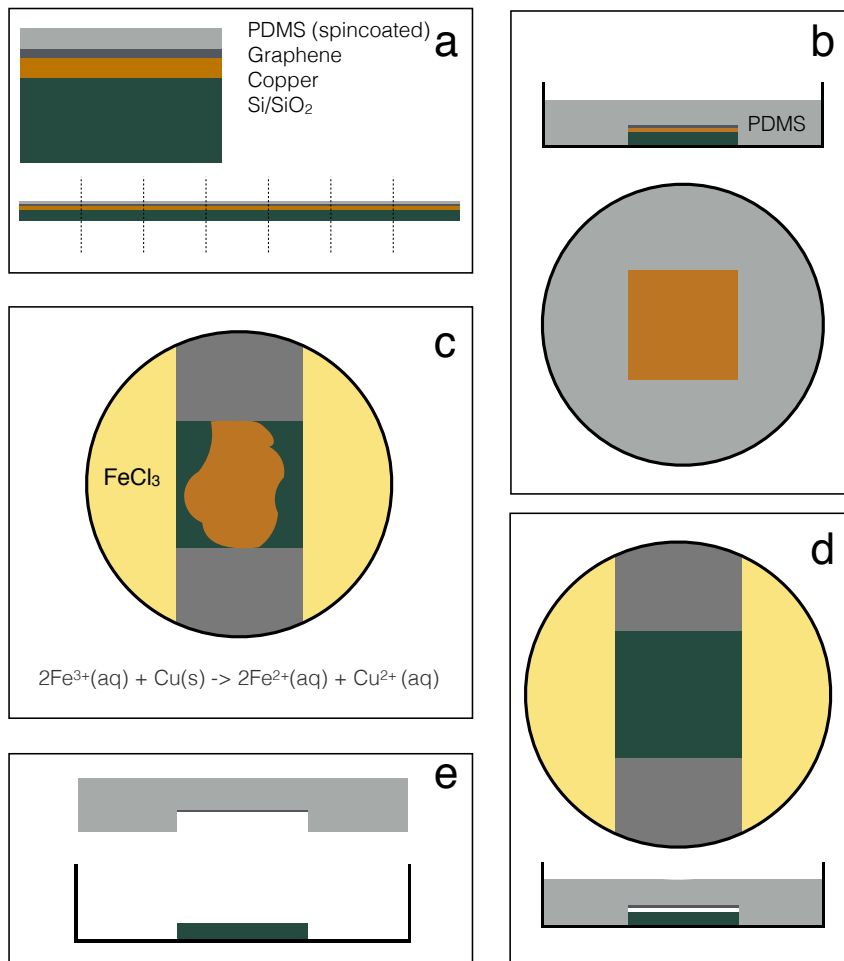


Figure 4.5: a) Spin coating a protective layer of liquid PDMS followed by dicing the wafer after curing of the PDMS. b) Pouring the bulk liquid PDMS in a Petri dish. c) After curing, parts of the PDMS are cut away, exposing the Cu from the sides, FeCl₃ is added to solve the Cu. d) When all copper is removed, the underlying SiO₂ is fully exposed. e) The PDMS-graphene substrate is lifted out of the Petri dish and cleaned thoroughly with DI water

4.3.3 Strain

Strain was exerted on the PDMS sample with a home made device as depicted in Figure 4.6. The substrate was clamped at both sides and strained by a linear stage (Thorlabs) with a displacement resolution of 10 μm. It is expected that strain transfer from the PDMS to the graphene is not perfect, but exact numbers are unknown and depending on the transfer process. Therefore, a range of strain increments is used in different experiments. Expected is a monotonical increase of the graphene strain with respect to the substrate strain, followed an asymptote; at high values of strain the Van Der Waals

forces will not be able to withstand the shear force that is required to strain the graphene further.

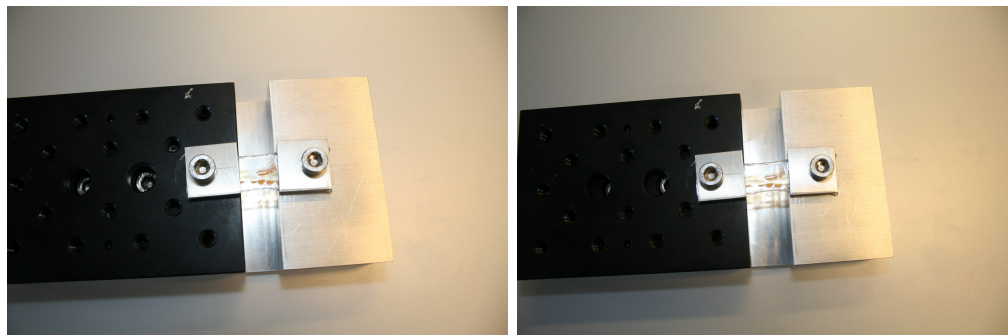


Figure 4.6: Tensile tester exerting strain on PDMS with graphene monolayer

Straining the PDMS causes physical transformation of the substrate, which means that the measurement location has to be revisited manually after each strain increment. This could pose a threat to the accuracy of the measurements; a change in peak location could be caused by a poor manual control instead of the straining of graphene. Also, it is expected that the graphene will not be strained (equally or at all) at each location: the stretching of PDMS could cause isotropic strain or pure translation on parts where the graphene is not well attached to the PDMS. To take these two issues into account, measurements are taken three times at two different locations at each strain setting to map the spatial sensitivity and show them in the form of error bars.

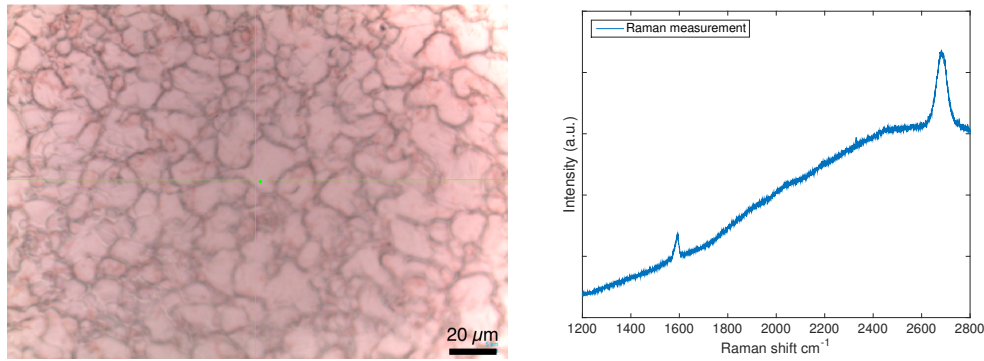
4.4 Results and discussion

This section describes the results and analysis of the production process of the stretchable graphene electrode as described in Section 4.3. A division is made into four parts: an inspection of the graphene before transfer, results of the transfer, evaluation of the sample when clamped, and finally the straining test.

4.4.1 Pre-transfer characterisation CVD graphene

The graphene was first inspected using optical microscopy and Raman spectroscopy for characterisation and future reference. Optical inspection shows the crystallites that are naturally present in copper, clearly visible because of the translucency of graphene (Figure 4.7a). Raman spectroscopy confirms the presence of graphene on the copper surface, characterised by the presence of the G and 2D band at a frequency of $\sim 1589\text{ cm}^{-1}$ and $\sim 2683\text{ cm}^{-1}$ respectively, as seen in Figure 4.7b.

Raman spectra were acquired at various, arbitrarily chosen locations and peak properties were obtained with Lorentzian fits. As these fits will be used to quantify the strain in



(a) Optical image of the copper-graphene substrate (b) Typical raman spectrum of graphene on a Cu foil

Figure 4.7

future experiments they were analysed in detail, from which the following information was extracted:

1. The D band at 1350 cm^{-1} is virtually absent at all spectra
2. The mean G band frequency is 1589.0 cm^{-1} with a standard deviation of 2.2 cm^{-1}
3. The mean 2D band frequency is 2683.1 cm^{-1} with a standard deviation of 2.9 cm^{-1}
4. The mean I_{2D}/I_G ratio is 1.80 with a standard deviation of 0.358

From point 1 it can be concluded that virtually no defects were present at the measurement locations, as seen by the absence of a peak at of $\sim 1350\text{ cm}^{-1}$. This means that measurements were taken mostly at the basal planes of the graphene lattice, where no defects are present, as opposed to edge sites. Unfortunately, due to the randomness of the measurement locations and small sample size, no definite statements can be made regarding the grain size, except for that grains can easily be found with dimensions greater than $0.5\text{ }\mu\text{m}$, which is the laser spot size of the spectroscope.

The I_{2D}/I_G ratio is used to identify the number of layers of graphene and shows that most locations contain monolayers ($I_{2D}/I_G > 1$), although some contain dual layers ($I_{2D}/I_G \approx 1$). Few layer graphene ($I_{2D}/I_G < 1$) was not found at the measurement locations.

4.4.2 Transfer

ME graphene The transfer was done according to the protocol in Paragraph 4.3.2, typical results from a transfer can be seen in Figure 4.8.

As can be seen from the images, some graphite flakes stuck to the PDMS and some remained on the silicon substrate. On a PDMS substrate graphene is practically invisible, however, from the before- and after pictures of the Silicon substate it was possible to find

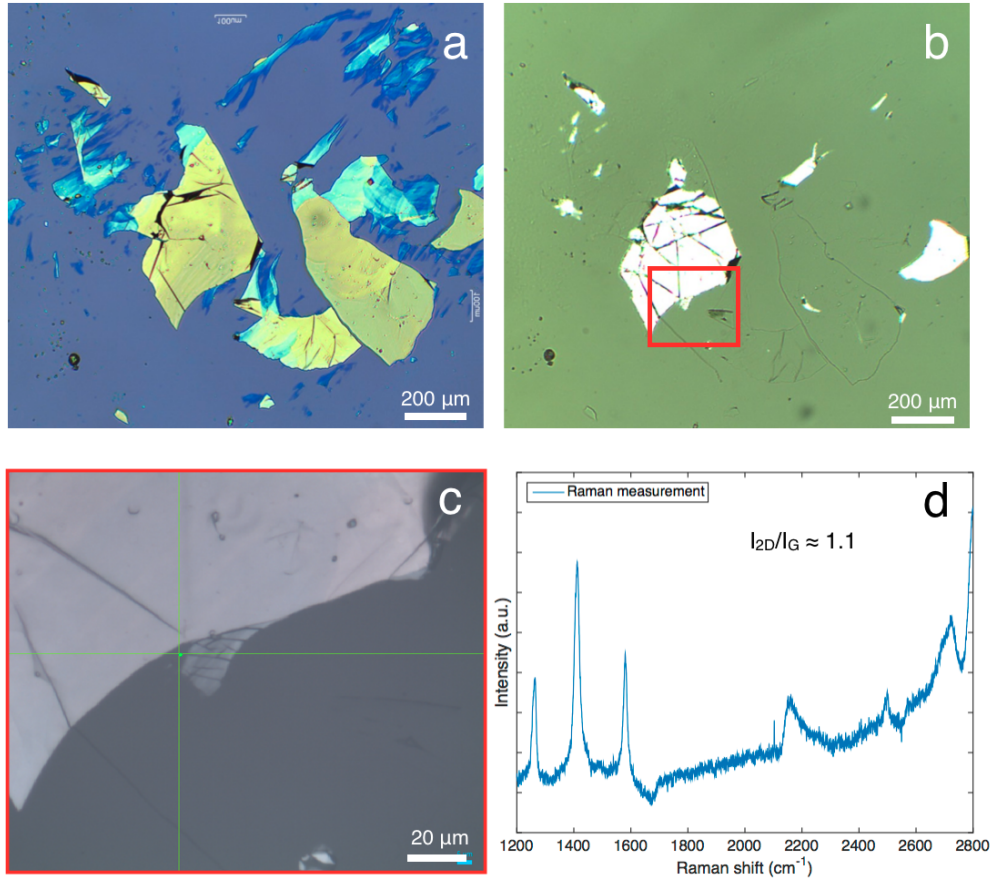


Figure 4.8: a) Graphite and graphene flakes on the Silicon substrate. b) Graphite and graphene flakes on the PDMS substrate after transfer (mirrored for clarity). c) Image of the Raman measurement location. Note that graphene is not visible on PDMS. d) Raman spectrum of the graphene confirms the presence of (dual layer) graphene

the locations where graphite was transferred, which serves as a reference point. After locating this exact flake on the PDMS, neighbouring sites are scanned on the before- and after pictures of the silicon substrate to find locations where graphene *might* have been transferred. Raman spectroscopy confirms the presence of graphene and evaluate the amount of layers present. In Figure 4.8d, a spectrum is shown where graphene was found. Although it was possible to find dual layer graphene (DLG), the lack of control over the quantity and locations of FLG or MLG make this method very laborious and time-consuming. However, due to the origin of the flakes, the flakes found are single crystalline (see Section 2.1).

CVD graphene The transfer was executed according to the protocol described in Section 4.3 with a few improvements after each iteration. Inspection was done using optical microscopy and Raman spectroscopy.

Visual inspection of the PDMS-graphene slab resulting from the first batch of transfers showed various kinds of contamination as shown in Figure 4.9.

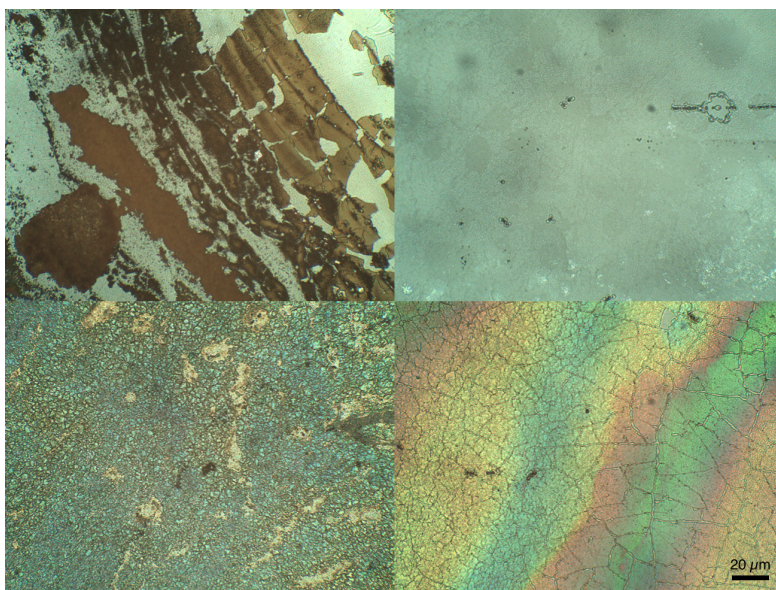


Figure 4.9: Overview of microscope images of the PDMS slab at various location after the first transfer process of graphene

Raman measurements show only graphene presence at the top-right image of Figure 4.9; it seems that at the other locations contaminations adhere to the PDMS and prevent the transfer of graphene. This was attributed to the heating of the sample during etching, causing water to evaporate and residues of Iron(III)chloride and Copper(II)chloride to adhere to the PDMS.

To reduce contaminations for further experiments, etching was performed at room temperature and while the etching time increased dramatically from ~ 2 days to ~ 10 days, contaminations were reduced, as seen in Figure 4.10.

Raman spectroscopy was done at various locations on the unclamped PDMS-graphene slab to map the presence of graphene and the variance of the G and 2D band frequency across the surface, from which the following information was extracted:

1. Graphene has not been transferred everywhere, still absent at locations where contaminations are present
2. The D band at 1350 cm^{-1} is still hardly visible
3. The mean G band frequency is 1583.91 cm^{-1} with a standard deviation of 2.70 cm^{-1}
4. The mean 2D band frequency is 2693.6 cm^{-1} with a standard deviation of 1.96 cm^{-1}

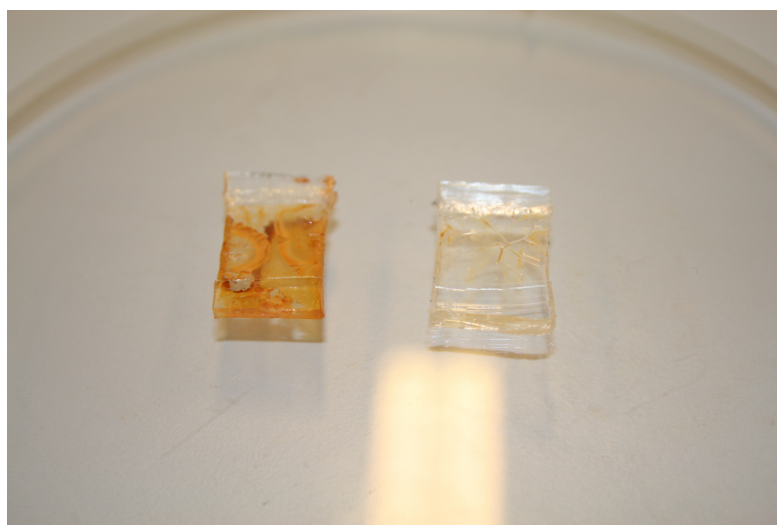


Figure 4.10: Photo showing decrease of contamination when etching at room temperature.

From the increase of the 2D band Raman shift it can be concluded that the graphene has been compressed during the transfer. This could have been expected as PDMS is known to shrink when curing[30], which has taken place twice during the transfer process. An increase of the 2D band frequency of 10.5 cm^{-1} corresponds to a strain of -0.15% , using a shift rate of $72 \text{ cm}^{-1}/\%$ [7] which is attributed to the polymerisation process of the PDMS.

4.4.3 Intermediate conclusion

The transfer methods corresponding to the two graphene sources were both successful, each with their own issues. An intermediate evaluation marks a milestone in the project; with which graphene source will the strain experiments be done?

Considering the ME graphene, transfer was possible but limited by the time available to the researcher. Several conclusions are made regarding this method:

1. The transfer process gives large uncertainties over the location and number of layers of the graphene transferred.
2. Time-consuming and strenuous work is required to locate flakes on the PDMS.
3. The yield of single crystalline flakes is relatively high.

Furthermore, designing an experiment for the ME graphene as an electrode would require building a new setup, using a micro electrochemical cell, costing considerable time. Although the decision is made to let it fall outside of the scope of this thesis, a preliminary outlook of the experiment can be found in Chapter 5.

Regarding the transfer of CVD graphene from a Cu substrate:

1. The transfer process of CVD graphene gives consistent results.
2. Contamination of the PDMS, preventing graphene from adhering is an issue.
3. The graphene is slightly compressed during the transfer due to the polymerisation of the PDMS.

Another disadvantage of the use of CVD graphene is the unknown behaviour of the grain boundaries under strain (see Section 2.3); this could obscure the influence of strain on its electroactivity. ME graphene, on the other hand, would reflect the influence of strain on its electrochemical response better.

The decision is made to continue with CVD graphene, mainly because of time constraints. Admittedly, ME graphene can yield results of higher quality but would require an electrochemical setup capable of working at a micrometer scale, in addition to the extra time required for the transfer. The main implication of this choice is that electrochemical microscopy is not required and the setup of Chapter 3

4.4.4 Clamping

The final goal of the thesis is to apply strain to the graphene and using it as an electrode during different strain settings. In the method chosen in this here, strain is not applied directly to the graphene but to a PDMS substrate with a layer of CVD graphene attached to it. The interfacial stress transfer is dependant on the van der Waals forces between the PDMS substrate and the graphene sheet and is expected to be less than 100%. Furthermore, a maximum strain is expected after which the graphene starts to slip and not follow the strain of the underlying substrate. Before straining the PDMS, Raman spectroscopy was performed on the clamped, unstrained graphene.

1. The D band at 1350 cm^{-1} is still hardly visible
2. The mean G band frequency is 1584.1 cm^{-1} with a standard deviation of 1.79 cm^{-1}
3. The mean 2D band frequency is 2692.2 cm^{-1} with a standard deviation of 4.32 cm^{-1}

Interestingly, the 2D band peak varies significantly more than before across the surface as seen from the standard deviation, which has more than doubled after clamping. As the 2D band frequency is directly related to the strain in the graphene lattice, it seems that extra tension and compression have been introduced in the sample. This is believed to be an consequence of the rubber-like nature of PDMS; clamping compresses and deforms the polymer locally and introduces inhomogeneous stresses across the surface, which are passed on to the graphene lattice. This has been taken into account for further experiments by carefully monitoring the measurement location.

Furthermore, clamping the sides of the sample induces out-of-plane buckling which has to be compensated by increasing the distance between the clamps, a process that is prone to manual errors. This process was improved by putting markers on the substrate and making sure their separation is kept equal after clamping. A small adjustment is

done to the clamping device to decrease compression caused by the clamps as seen in Figure 4.11.

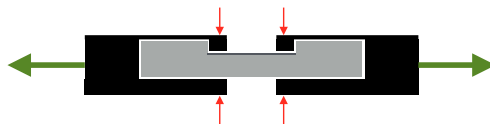


Figure 4.11: Schematic of the clamping system: red arrows indicate clamping forces, green arrows show the direction of strain

4.4.5 Strain

The last step before performing the electrochemical experiments on strained graphene is the matching of the strain exerted on the PDMS to that in the graphene lattice.

Strain was exerted on different samples, with varying strain increments, as applied to the PDMS. From the spectra, shown in Figure 4.12 until 4.13, the 2D band shift is extracted and plotted against the strain applied to the PDMS.

In the results of Figures 4.12-4.13, there seem to be two issues that prevent the observation of a trend that can be used to learn more about the graphene-PDMS interface:

Location-dependant strain distribution There is a location-dependant, inhomogeneous stress distribution over the surface caused by the clamping of the substrate. In combination with the manual positioning of the Raman laser spot, a high variation of strain is seen. In order to reduce this variation, multiple measurements were done at each location to be able to map the spatial sensitivity of the 2D band peak location. This stress variation could be amplified by the imperfect uniaxial strain on the PDMS.

In the measurement of Figure 4.12c, the standard deviation was kept relatively low at location 1, even reaching 0 cm^{-1} after the second strain increment with an average of 0.2689 cm^{-1} ; this was done by carefully controlling the measurement position. Nevertheless, because of the larger deviation at other measurements, a trend curve still could not be fitted, which can be attributed to the second issue.

Weak interfacial stress transfer It is expected that stress is transferred imperfectly from the PDMS slab to the graphene lattice. Bisset et al. report a maximum PDMS-induced strain of around 0.2-0.3% (graphene value) and a poor interfacial stress transfer in general[7]. However, they were able to measure an upshift of the 2D band frequency, albeit poor, with an order of magnitude difference with respect to the PDMS strain. This could explain the difficulty of finding a relationship between the PDMS strain and graphene 2D peak shift. Possible causes for this extraordinarily weak transfer:

1. The graphene is loosely attached to the PDMS, causing slippage when the PDMS is strained; translation and tear as opposed to deformation.

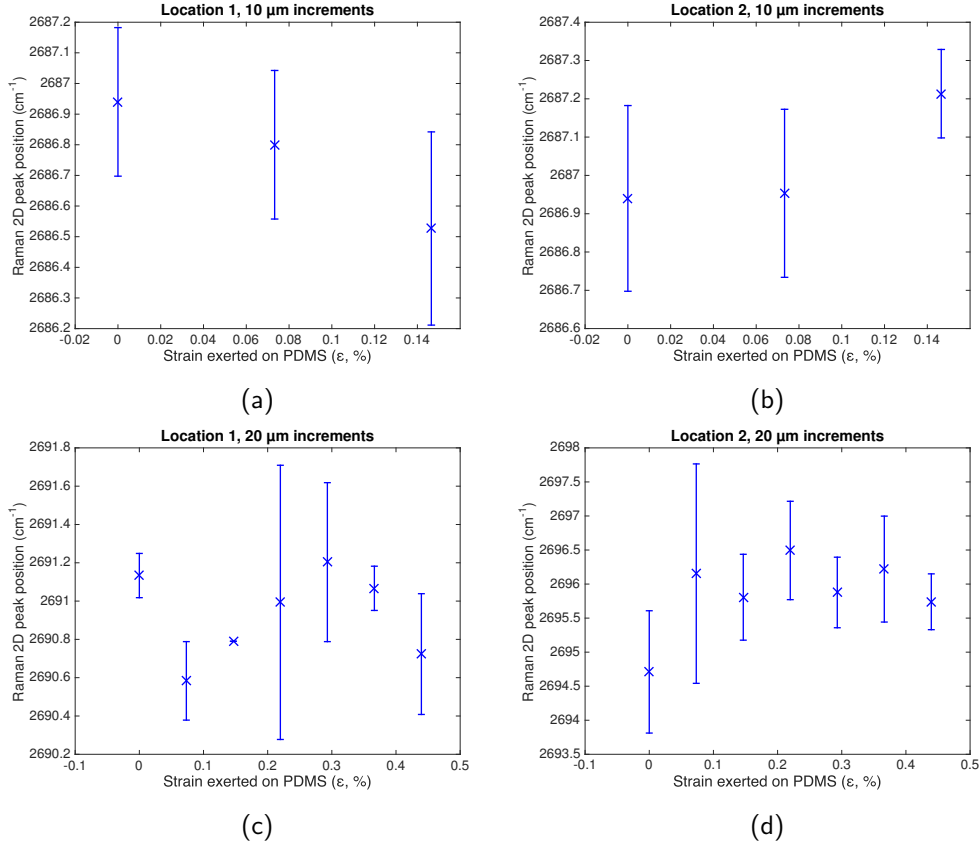


Figure 4.12: 2D band frequency shift upon strain with increments of 10 and 20 μm at two different locations in the graphene lattice. Crosses mark individual results, error bars show standard deviations.

2. Surface roughness, originating from the copper grains and imprinted on the PDMS cause corrugations in the graphene lattice and prevent stress from being distributed across the surface. The graphene is being 'de-wrinkled'.
3. Grain boundaries break at relatively low stress levels and cause the formation of grain 'islands', moving apart but staying undeformed.

Another possible explanation for the absence of a clear trend is the inhomogeneous strain distribution of the PDMS at a scale that is smaller than the Raman spectroscopy laser spot size, due to the Poisson's ratio of PDMS, which is measured to be 0.5 and the imperfect uni-axially applied strain. This could cause tension between some carbon atoms and compression between others but when measuring the bulk surface averaging to an unaffected peak shift. A broadening of the 2D peak should reflect this variation of strain within a measurement. However, broadening was not observed when analysing the relationship between applied strain and the full width at half maximum value of the 2D peak and is thus assumed to be untrue.

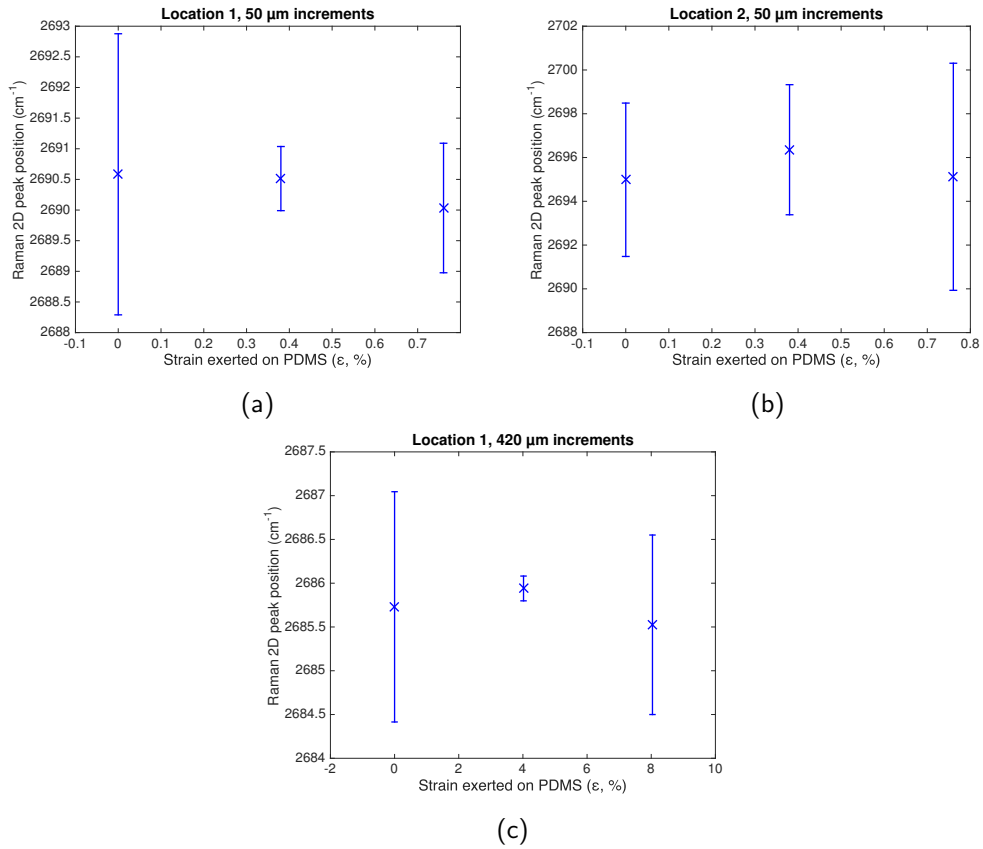


Figure 4.13: 2D band frequency shift upon strain with increments of 50 and 420 μm at two different locations in the graphene lattice. Crosses mark individual results, error bars show standard deviations.

Final experiment improvements After the tests shown above, the measurement location was taken more carefully and clamping was improved by changing the clamps as shown in Figure 4.11 which required less clamping force which decreased warping of the substrate. Also, it was decided to only measure wavenumbers within the vicinity of the 2D peak, thereby losing supervision of the D and G peak. Thus, the introduction of defects could not be monitored but the measurement time was decreased by a factor of four (from 20 min to 5 min).

After increasing the amount of strain even further, up to 22.5%, a trend could be observed. Looking at Figure 4.14, one can roughly observe a decreasing regime and a maximum strain. After this maximum, the Van Der Waals forces are not able to transfer the strain to the graphene anymore. This maximum seems to be different for different locations, which is expected because of the inhomogeneous morphology of the PDMS substrate. The maximum amount of strain achieved is at the measurement of

Figure 4.14, which is 0.03 % to 0.17 %, calculated with the shift-per-strain values found in literature (see Subsection 4.3.1). This value corresponds to the value found in literature of 0.2 % to 0.3 % [7]. The corresponding maximum 2D peak shift is 1.71 cm^{-1} . Only the two locations at which the highest peak shift was measured are shown here; a third location was measured at which the 2D peak shift was only minimal.

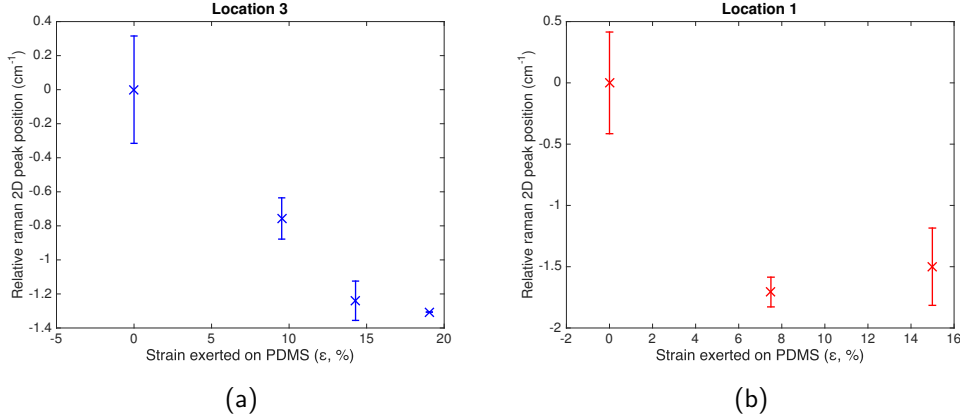


Figure 4.14: 2D band frequency shift upon large strain of two different samples. Crosses mark individual results, error bars show standard deviations of three measurements.

4.5 Summary and conclusion

In this chapter a stretchable graphene electrode was designed, produced and tested.

Two types of graphene were transferred to a polydimethylsilyoxane (PDMS) substrate: mechanically exfoliated (ME) graphene and copper-grown chemical vapour deposition (CVD) graphene. Existing transfer methods were modified to fit the application in question but after transferring ME graphene to PDMS it was decided to not continue with this source of graphene: the process was time-consuming and highly stochastic in terms of successful yield. Transfer of CVD graphene proved to be a more reliable method to transfer graphene to a flexible substrate but required a long waiting period of about 10 d to 15 d. A small compression was observed on the surface after the transfer, attributed to PDMS shrinkage during curing, as well as introduction of an inhomogeneous stress distribution as a result of clamping.

Strain was applied using a simple tensile clamping device after which the graphene strain was measured with Raman spectroscopy, using its ω_{2D} -strain relation. The location of measurement turned out to be extremely important resulting in high variability of peak position. Meticulous control of measurement location had to be taken to overcome this variability. Eventually, at PDMS strain levels of 0 % to 15 %, graphene strain was found up to $\sim 0.17\%$ which equates to an interfacial stress transfer of $\epsilon_{\text{graphene}}/\epsilon_{\text{PDMS}} = 2 \times 10^{-3}$ to 11.3×10^{-3} .

5 Conclusions and recommendations

An investigation has been done exploring the possibility to use strain to chemically tune graphene, such that it becomes more receptive to covalent bonds on its surface. This is a relatively new field because up until now, most of the strain engineering of graphene was directed towards the generation of a band gap and the specific adsorption of atomic hydrogen for energy storage. The experience gained and reported in this document can be used to research how specific species can be adsorbed by graphene with the help of strain.

5.1 Conclusions

A literature study has been done in which the mechanism behind strain-induced increase of reactivity was investigated. Graphene from two different production methods were considered, of which mechanically exfoliated (ME) graphene was found to be the best candidate in terms of quality. However, graphene produced through chemical vapour deposition (CVD) would be easier to handle because of its larger possible size. Uni-axial strain is required to shift the electronic structure such that the graphene become more susceptible to covalent bonds. The quantity of strain required depends on the species that will functionalise the surface. Research regarding the electrochemical behaviour of graphene has shown some contradicting results, but most importantly, the basal plane of graphene is electroactive, as opposed to previous predictions. The introduction of electrochemical microscopy has given new information by decreasing the electrode-electrolyte interface immensely.

An electrochemical setup was designed and built that was able to do electrochemistry in a drop and was tested using graphite and CVD graphene on a Si/SiO₂ substrate. The minimum achieved reaction area was in the millimetre range. The coverage of CVD graphene was found to be limiting the contact area and influence of unwanted reactions proved to be overshadowing the cathodic and anodic peaks at the electrode interface.

An approach was taken that used a flexible substrate to strain graphene. Both ME and CVD graphene were transferred to a polydimethylsiloxane (PDMS), the transfer of CVD graphene was found to be more reliable. Measurable strain was found to be difficult to achieve but successful after various improvements of the transfer, strain application and

measurement method. A maximum 2D peak Raman shift, a well-known method to measure strain in graphene, of 1.71 cm^{-1} , corresponding to a graphene strain of 0.17 % to 0.03 %.

Unfortunately, the research question has not been answered. An approach was taken that divided the question into two parts, but the assembly of these two techniques is missing. However, both techniques are proven to work, and new, simple methods are demonstrated that are able to do electrochemistry in a droplet and transfer graphene to a flexible substrate.

5.2 Outlook

There are a lot of actions to be taken in order to use graphene as a sensor material. First of all, the setup described in this document should be used to characterise the electrochemical change of graphene upon strain. The experiment that was planned originally for this project is described in Appendix E and should be the next step when this research is continued.

If it is proven that strain can significantly improve the electroactivity of graphene, one can start to look at specific molecules that, at a specific strain setting, can be adsorbed by the lattice. Surface modification can be done through a technique called electrografting. This would not deteriorate the electrical conductivity as much as the chemical reduction of graphite oxide, the current way to produce graphene-based (electrochemical) sensors (see Section 2.1).

Another challenge is the integration of the functionalised graphene in the application of choice. One could imagine, for example, modified graphene surfaces with species that detect water molecules, temperature increases and the presence of smoke. These can be scaled down, with a low power consumption, such that the whole system can be incorporated in a sticker that can be placed on a wall. This is communicated to a mainframe (Bluetooth 4.0 is already incorporated in stickers). With this information room temperature can be controlled, a sudden increase in humidity can be monitored and emergency services can be notified in case of fire. This is but one of the numerous examples which shows how graphene-based sensors can help to create a world with ‘smart’ objects, a futuristic vision known as the Internet of Things.

Bibliography

- [1] P L De Andres and J A Vergés. First-principles calculation of the effect of stress on the chemical activity of graphene. *Applied Physics Letters*, 171915(2008):1–4, 2008.
- [2] Craig E Banks, Trevor J Davies, Gregory G Wildgoose, and Richard G Compton. Electrocatalysis at graphite and carbon nanotube modified electrodes : edge-plane sites and tube ends are the reactive sites. *The Royal Society of Chemistry*, pages 829–841, 2005.
- [3] Allen J. Bard and Larry R. Faulkner. *Electrochemical methods : fundamentals and applications*. John Wiley & Sons, Inc, 2001.
- [4] Daniel Belanger and Jean Pinson. Electrografting: a powerful method for surface modification. *Chem Soc Rev*, 40:3995–4048, 2011.
- [5] James J. van Benschoten, Jane Y. Lewis, and William R. Heineman. Cyclic voltammetry. *Journal of Chemical Education*, 60(9):702, 1983.
- [6] Mark A Bissett. Enhanced Chemical Reactivity of Graphene Induced by Mechanical Strain. *ACS Nano*, (February 2016), 2013.
- [7] Mark A Bissett, Wataru Izumida, Riichiro Saito, and Hiroki Ago. Supporting Information Effect of Domain Boundaries on the Raman Spectra of Mechanically Strained Graphene. *ACS Nano*, 2:1–12, 2012.
- [8] Hanns-Peter Boehm. Graphene: How a laboratory curiosity suddenly became extremely interesting. *Angewandte Chemie International Edition*, 49(49):9332–9335, 2010.
- [9] Robert J Bowling, Richard T Packard, and Richard L McCreery. Activation of Highly Ordered Pyrolytic Graphite for Heterogeneous Electron Transfer : Relationship between Electrochemical Performance and Carbon Microstructure. *J. Am. Chem. Soc.*, (24):1217–1223, 1989.
- [10] Dale a. C. Brownson and Craig E. Banks. *The Handbook of Graphene Electrochemistry*. Number Cvd. 2014.

- [11] Kemal Celebi. *Chemical Vapor Deposition of Graphene on Copper*. PhD thesis, ETH Zurich, 2013.
- [12] Seon-Myeong Choi, Seung-Hoon Jhi, and Young-Woo Son. Effects of strain on electronic properties of graphene. *Phys. Rev. B*, 81:081407, Feb 2010.
- [13] Trevor J. Davies, Michael E. Hyde, and Richard G. Compton. Nanotrench arrays reveal insight into graphite electrochemistry. *Angewandte Chemie - International Edition*, 44(32):5121–5126, 2005.
- [14] Fei Ding, Hengxing Ji, Yonghai Chen, Andreas Herklotz, Kathrin Do, Yongfeng Mei, Armando Rastelli, and Oliver G Schmidt. Stretchable Graphene : A Close Look at Fundamental Parameters through Biaxial Straining. *Nano Letters*, (10):3453–3458, 2010.
- [15] M.S. Dresselhaus, Dresselhaus G., and J.E. Fischer. Graphite intercalation compounds: Electronic properties in the dilute limit. *Physical Review B*, 15(6), 1977.
- [16] M. Eizenberg and J.M. Blakely. Carbon monolayer phase condensation on ni(111). *Surface Science*, 82(1):228 – 236, 1979.
- [17] Centre for Astrophysics and University of Kent Planetary Science. Raman spectroscopy scattering scenarios. http://astro.kent.ac.uk/research/research_mjb/raman.html, 2016. [Online; accessed 11-September-2016].
- [18] Neil Gross. The Earth Will Don an Electric Skin. *Business Week*, page 134, August 1999.
- [19] Aleix G Guell, Neil Ebejer, Michael E Snowden, Julie V Macpherson, and Patrick R Unwin. Structural Correlations in Heterogeneous Electron Transfer at Monolayer and Multilayer Graphene Electrodes. *Journal of the American Chemical Society*, (134):7258–7261, 2012.
- [20] Yuan Huang, Eli Sutter, Norman N Shi, Jiabao Zheng, Tianzhong Yang, Dirk Englund, Hong-jun Gao, and Peter Sutter. Reliable Exfoliation of Large-Area High-Quality Flakes of Graphene and Other Two-Dimensional Materials. *ACS Nano*, 9(11):10612–10620, 2015.
- [21] Kristin R Kneten and Richard L McCreery. Effects of Redox System Structure on Electron-Transfer Kinetics at Ordered Graphite and Glassy Carbon Electrodes. *Analytical Chemistry*, (64):2518–2524, 1992.
- [22] Tapas Kuila, Saswata Bose, Ananta Kumar, and Partha Khanra. Progress in Materials Science Chemical functionalization of graphene and its applications. *Progress in Materials Science*, 57(7):1061–1105, 2012.
- [23] Stanley C S Lai, Anisha N Patel, Kim M Kelvey, and Patrick R Unwin. Definitive Evidence for Fast Electron Transfer at Pristine Basal Plane Graphite from High-Resolution Electrochemical Imaging. *Angewandte Chemie*, (51):5405–5408, 2012.

- [24] Changgu Lee, Xiaoding Wei, Jeffrey W Kysar, and James Hone. Measurement of the Elastic Properties and Intrinsic Strength of Monolayer Graphene. *Science*, 321:385–388, 2008.
- [25] Jing Li, Xuan-Yun Wang, Xing-Rui Liu, Zhi Jin, Dong Wang, and Li-jun Wan. Facile growth of centimeter-sized single-crystal graphene on copper foil at atmospheric pressure. *Journal of Materials Chemistry C*, 3(15):3530–3535, 2015.
- [26] Wan Li, Cen Tan, and Michael a Lowe. Electrochemistry of Individual Monolayer Graphene Sheets. *ACS Nano*, 5(3):2264–2270, 2011.
- [27] Kian Ping Loh, Qiaoliang Bao, Priscilla Kailian Ang, and Jiaxiang Yang. The chemistry of graphene. *J. Mater. Chem.*, (20):2277–2289, 2010.
- [28] Chun-hua Lu, Huang-hao Yang, Chun-ling Zhu, Xi Chen, and Guo-nan Chen. A Graphene Platform for Sensing Biomolecules. *Angewandte Chemie*, (48):4785–4787, 2009.
- [29] Gary A Mabbott. An Introduction to Cyclic Voltammetry. *Journal of Chemical Education*, 60(9):697–702, 1983.
- [30] Morten Hannibal Madsen, Nikolaj A Feidenhans, and Poul-erik Hansen. Accounting for PDMS shrinkage when replicating structures. *J. Micromech. Microeng.*, 127002, 2014.
- [31] MatWeb material database. Searchable database of material properties. <http://www.matweb.com/search/DataSheet.aspx?MatGUID=d1844977c5c8440cb9a3a967f8909c3a&ckck=1>, 2016. [Online; accessed 13-september-2016].
- [32] Cecilia Mattevi and Manish Chhowalla. A review of chemical vapour deposition of graphene on copper. *Journal of Materials Chemistry*, (21):3324–3334, 2011.
- [33] Richard L Mccreery. Advanced Carbon Electrode Materials for Molecular Electrochemistry. *Chem. Rev.*, pages 2646–2687, 2008.
- [34] A.D. McNaught, A. Wilkinson, International Union of Pure, and Applied Chemistry. *Compendium of Chemical Terminology: IUPAC Recommendations*. IUPAC Chemical Data Series. Blackwell Science, 1997.
- [35] T. M G Mohiuddin, a. Lombardo, R. R. Nair, a. Bonetti, G. Savini, R. Jalil, N. Bonini, D. M. Basko, C. Galiotis, N. Marzari, K. S. Novoselov, a. K. Geim, and a. C. Ferrari. Uniaxial strain in graphene by Raman spectroscopy: G peak splitting, Grüneisen parameters, and sample orientation. *Physical Review B - Condensed Matter and Materials Physics*, 79(20):1–8, 2009.
- [36] A.E. Morgan and G.A. Somorjai. Low Energy Electron Diffraction Studies of Gas Adsorption on the Platinum (100) Single Crystal Surface. *Surface Science*, 12:405–425, 1968.

- [37] A H Castro Neto. The electronic properties of graphene. *Reviews of Modern Physics*, 81, 2009.
- [38] Zhen Hua Ni, Ting Yu, Yun Hao Lu, Ying Ying Wang, Yuan Ping Feng, and Ze Xiang Shen. Uniaxial strain on graphene: Raman spectroscopy study and band-gap opening. *ACS Nano*, 2(11):2301–2305, 2008.
- [39] K S Novoselov, A K Geim, S V Morozov, and D Jiang. Electric Field Effect in Atomically Thin Carbon Films. *Science*, 306(October):666–669, 2004.
- [40] K. S. Novoselov, D. Jiang, F. Schedin, T. J. Booth, V. V. Khotkevich, S. V. Morozov, and A. K. Geim. Two-dimensional atomic crystals. *Proceedings of the National Academy of Sciences of the United States of America*, 102(30):10451–10453, 2005.
- [41] K S Novoselov, Z Jiang, Y Zhang, S V Morozov, H L Stormer, U Zeitler, J C Maan, G S Boebinger, P Kim, and A K Geim. Room-Temperature Quantum Hall. *Science*, 315(March):2007, 2007.
- [42] Anisha N Patel, Manon Guille Collignon, Michael A O Connell, Wendy O Y Hung, Kim Mckelvey, Julie V Macpherson, and Patrick R Unwin. A New View of Electrochemistry at Highly Oriented Pyrolytic Graphite. *J. Am. Chem. Soc.*, (134):20117–20130, 2012.
- [43] B Paulchamy, G Arthi, and Lignesh Bd. A Simple Approach to Stepwise Synthesis of Graphene Oxide. *Nanomedicine and Nanotechnology*, 6(1):2–5, 2015.
- [44] Vitor M. Pereira, a. H. Castro Neto, and N. M R Peres. Tight-binding approach to uniaxial strain in graphene. *Physical Review B - Condensed Matter and Materials Physics*, 80(4):1–9, 2009.
- [45] H. Hugo Pérez Garza, Eric W. Kievit, Grégory F. Schneider, and Urs Staufer. Controlled, reversible, and nondestructive generation of uniaxial extreme strains (>10%) in graphene. *Nano Letters*, 14(7):4107–4113, 2014.
- [46] Héctor Hugo Pérez-Garza, Eric Walter Kievit, Grégory F Schneider, and Urs Staufer. Highly strained graphene samples of varying thickness and comparison of their behaviour. *Nanotechnology*, 25(46):465708, 2014.
- [47] Ioannis Polyzos, Massimiliano Bianchi, Laura Rizzi, Emmanuel N Koukaras, John Parthenios, Konstantinos Papagelis, Roman Sordan, and Costas Galiotis. Suspended monolayer graphene under true uniaxial deformation. *Royal Society of Chemistry*, pages 13033–13042, 2015.
- [48] MIT professional education. Artist’s impression of the internet of things. http://news.mit.edu/sites/mit.edu.newsoffice/files/styles/news_article_image_top_slideshow/public/images/2016/internet-of-things_0.png?itok=-ADYIV6n, 2016. [Online; accessed 13-September-2016].

- [49] Hyacinthe Randriamahazaka and Jalal Ghilane. Electrografting and Controlled Surface Functionalization of Carbon based Surfaces for Electroanalysis. *Electroanalysis*, (27):1–15, 2015.
- [50] R. M. Ribeiro, V. M. Pereira, N. M. R. Peres, P. R. Briddon, and A. H. Castro Neto. Strained graphene: tight-binding and density functional calculations. *New Journal of Physics*, 11(11):115002, November 2009.
- [51] P. Ruffieux, O. Gröning, M. Biemann, P. Mauron, L. Schlapbach, and P. Gröning. Hydrogen adsorption on sp²-bonded carbon: Influence of the local curvature. *Physical Review B*, 66(24):1–8, 2002.
- [52] Luigi Sasso. *Novel Materials for Cellular Nanosensors*. PhD thesis, DTU Nanotech - Department of Micro- and Nanotechnology, 6 2012.
- [53] F Schedin, a K Geim, S V Morozov, E W Hill, P Blake, M I Katsnelson, and K S Novoselov. Detection of individual gas molecules adsorbed on graphene. *Nature materials*, 6(9):652–655, 2007.
- [54] Chen Si, Zhimei Sun, and Feng Liu. Strain engineering of graphene : a review. *Royal Society of Chemistry*, pages 3207–3217, 2016.
- [55] Cen Tan, Joaquín Rodríguez-López, Joshua J Parks, Nicole L Ritzert, and Daniel C Ralph. Reactivity of Monolayer Chemical Imperfections Studied Using Scanning Electrochemical Microscopy. *ACS Nano*, (4):3070–3079, 2012.
- [56] Peter S. Toth, Anna T. Valota, Matej Velicky, Ian A. Kinloch, Kostya S. Novoselov, Ernie W. Hill, and Robert A. W. Dryfe. Electrochemistry in a drop: a study of the electrochemical behaviour of mechanically exfoliated graphene on photoresist coated silicon substrate. *Chem. Sci.*, 5:582–589, 2014.
- [57] Dissemination of IT for the Promotion of Materials Science University of Cambridge. Raman scattering. [http://www.doitpoms.ac.uk/tlplib/raman_scattering.php](http://www.doitpoms.ac.uk/tlplib/raman/raman_scattering.php), 2016. [Online; accessed 13-September-2016].
- [58] Anna T Valota, Ian A Kinloch, Kostya S Novoselov, Cinzia Casiraghi, Axel Eckmann, Ernie W Hill, and Robert A W Dryfe. Electrochemical Behavior of Monolayer and Bilayer Graphene. *ACS Nano*, (11):8809–8815, 2011.
- [59] Tijn van Omme. Optimized MEMS-based tensile devices towards the generation of extreme strain in CVD graphene. Master’s thesis, Delft University of Technology, the Netherlands, 2016.
- [60] Matej Velicky, Dan F Bradley, Adam J Cooper, Ernie W Hill, Ian A Kinloch, Artem Mishchenko, Konstantin S Novoselov, Hollie V Patten, Peter S Toth, Anna T Valota, Stephen D Worrall, and Robert A W Dryfe. Electron Transfer Kinetics on Mono- and Multilayer Graphene. *ACS Nano*, (10):10089–10100, 2014.

- [61] P R Wallace. The Band Theory of Graphite. *Physical Review*, 71(9), 1947.
- [62] Z F Wang, Yu Zhang, and Feng Liu. Formation of hydrogenated graphene nanoripples by strain engineering and directed surface self-assembly. *Physical Review B*, 041403(83):1–4, 2011.
- [63] Eric Whiteway, Wayne Yang, Victor Yu, and Michael Hilke. Time Evolution of the Growth of Single Graphene Crystals and High Resolution Isotope Labeling. *Unpublished*, 8, 2015.
- [64] Shixin Wu, Qiyuan He, Chaoliang Tan, Yadong Wang, and Hua Zhang. Graphene-Based Electrochemical Sensors. *Small*, (8):1160–1172, 2013.
- [65] Wenjing Yuan, Yu Zhou, Yingru Li, Chun Li, Hailin Peng, Jin Zhang, Zhongfan Liu, Liming Dai, and Gaoquan Shi. The edge- and basal-plane-specific electrochemistry of a single-layer graphene sheet. *Scientific Reports*, 3:2248, jul 2013.
- [66] Guohui Zhang, Anatolii S Cuharuc, Aleix G Gu, and Patrick R Unwin. Electrochemistry at highly oriented pyrolytic graphite (HOPG): lower limit for the kinetics of outer-sphere redox processes and general implications for electron transfer models . *Phy. Chem.*, pages 11827–11838, 2015.

A Electrochemistry basics

As this thesis is written for a degree in mechanical engineering rather than in chemistry, a brief introduction into the realm of electrochemistry will be given in this section which should cover the basics for the rest of the research. Needless to say, electrochemistry is the field of science which deals with electronics and chemistry. It involves chemical processes at the interface of an electrode and ionic conductor and the movement of electrons. This chemical process, a so-called redox reaction, is what lies at the heart of this field:



In essence, it consists of two concurring reactions: an oxidation (k_{ox}), denoted by the arrow pointing to the left, and a reduction (k_{red}), denoted by the arrow pointing to the right. O and R^{n-} are the oxidised and reduced forms of a substance in an aqueous media and n is an integer. Its quantity depends on the type of reaction. Oxidation removes an electron from the reduced form of the substance and reduction does the opposite to the oxidised form. Depending on the direction of the reaction, the electrons are either supplied or lead away through the electrode repeatedly, thus causing a current to flow. In this research, the focus will be on the redox reactions that are caused by the introduction of an electrical potential. As a consequence of this potential, charge is transported: in the electrode it is transported through the movement of electrons, in the electrolyte through the movement of ions.

The structure comprised by the electrode and the surrounding electrolyte (the redox couple) is called a half-cell and the electrode-electrolyte interface is separated by the Helmholtz double layer, in which the redox reactions take place.

Helmholtz double layer

The Helmholtz double layer arises naturally wherever redox reactions take place between an electrode and an electrolyte. It is a consequence of the electrostatic attractive forces between the electrons in the electrode and the charged species in the solution (in the vicinity of the electrode). In a half-cell, one can identify a region where most of the redox reactions take place. This region is called the Helmholtz double layer. The rates of the electrode processes are affected by the structure of the double layer that is formed in the solution close to the electrode[3].

A schematic drawing of this layer can be found in Figure A.1.

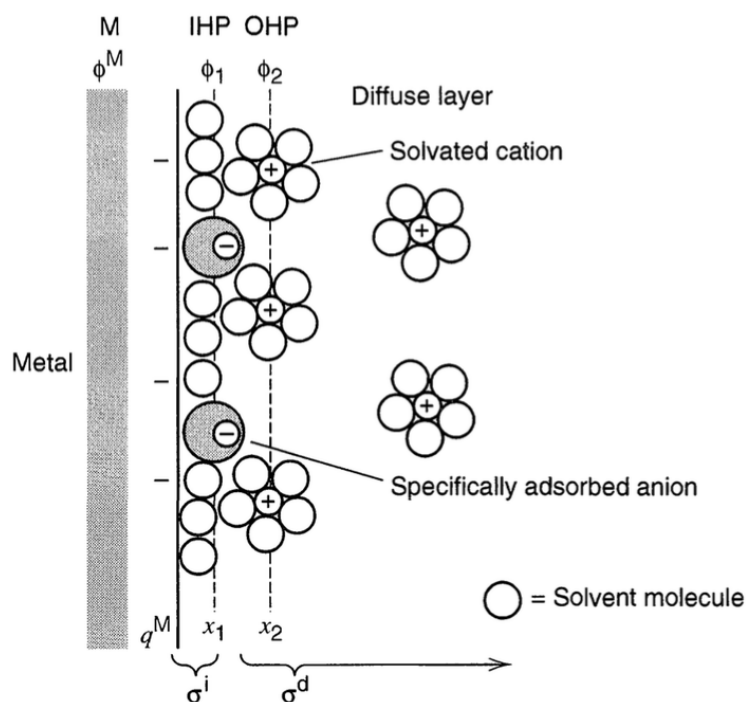


Figure A.1: Schematic representation of the composition of the electrical double layer [3]

Two layers are considered:

Inner Helmholtz plane (IHP) This is the region closest to the electrode which marks the inner plane of the Helmholtz layer. This layer contains the specifically adsorbed ions and their total charge density is σ^i ($\mu\text{C}/\text{cm}^2$).

Outer Helmholtz plane (OHP) The outer boundary surface of the Helmholtz layer marks the nearest location to the electrode for the solvated ions. At this distance long-range electrostatic forces predominate in the ion-electrode interaction; chemical reactions are said to be non-influential. These *nonspecifically adsorbed* ions are contained in the diffuse layer of the solution, which is bounded by the OHP and extends into the bulk of the solution. Their total charge density is σ^d .

The IHP and OHP can act like a capacitor, which is a factor that should be taken into account in this research.

A.0.1 Electrochemical analysis

There are several ways to perform electrochemical analysis; they can be grouped into three categories; potentiometry, coulometry and voltammetry. A extensive overview of

this can be found in Figure A.2.

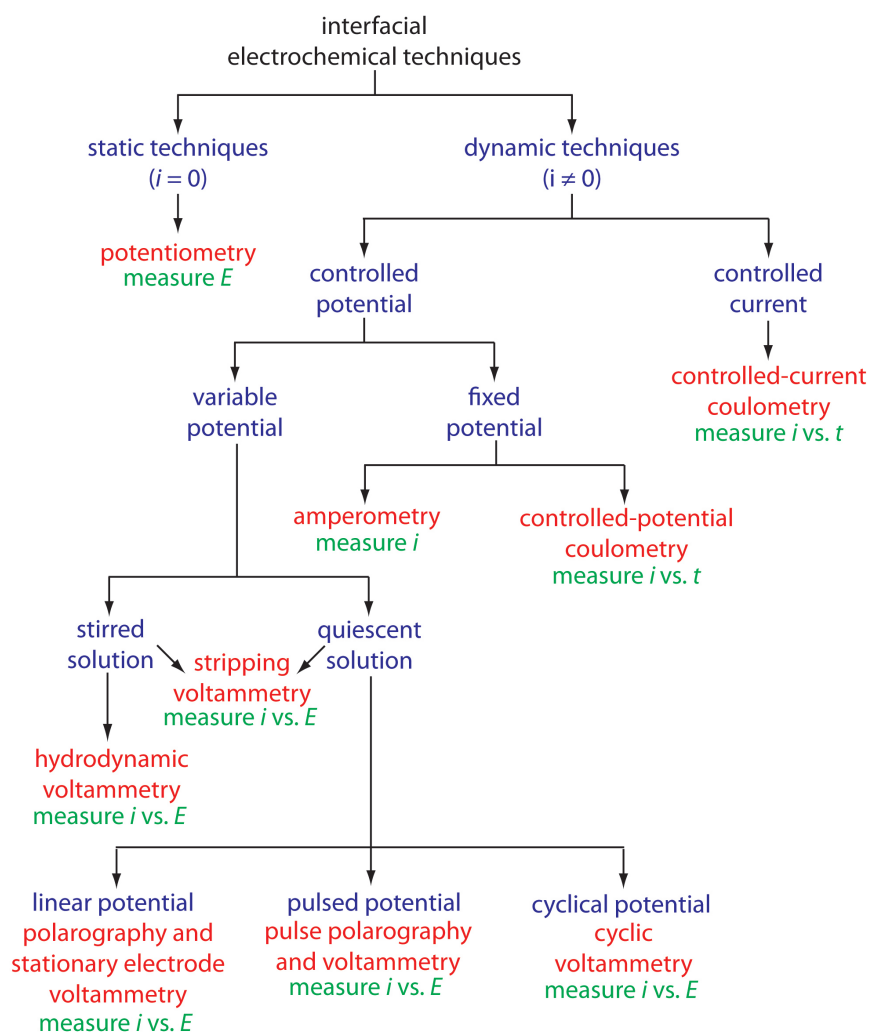


Figure A.2: Family tree with the most used interfacial electrochemical techniques. Specific techniques in red, experimental conditions in blue, analytical signals in green[5]

Potentiometry measures the potential of an indicator electrode without allowing any significant current to pass through the electrochemical cell. It is a static technique, and will therefore not be discussed in this proposal. Coulometric methods are based on Faraday's law to the effect that the total charge or current passed during electrolysis is proportional to the reactants and products in the redox reaction. Voltammetry measures the current in an electrochemical cell as a function of the applied potential.

Voltammetry

A popular way to study dynamic electrochemical properties in any substance or electrode is voltammetry, which consists of one half-cell. When doing voltammetry, a three electrode system is usually employed, all three of which are submerged in the half-cell liquid. A so-called working electrode (WE) drives the redox reactions (from equation A.0.1) in the liquid because a potential is applied to it with respect to a reference electrode (RE) which has a known and constant potential. No current should pass through the reference electrode. A third counter electrode (CE) is put in the solution to facilitate the supply and removal of electrons and completes the electrical circuit.

When a potential is applied between the RE and the WE, there will also be a potential difference between the CE and the WE. As seen in Figure A.1, the increased (or decreased) energy level of the electrons of the electrode material will cause reductive (or oxidative) reactions to take place in a thin layer around the electrode. This causes a current to flow to the counter electrode, or to the working electrode depending on the polarity of the potential. When the potential is increased, the current increases until the ions in the vicinity of the electrodes are depleted.

A potentiostat is used which acts as the interface between the half-cell and a computer. It has built-in electrode connections and the accompanying software has pre-set programs for the most frequently used measurements.

B Ag/AgCl reference electrode preparation

A silver wire (99.9%, 0.5mm diameter, Sigma Aldrich) was insulated with a pipette tip to keep the exposed area constant throughout all experiments. Superglue (cyanoacrylate) was used to fully insulate the wire/pipette interface such that no liquid enters the pipette (Figure B.2a).

Chlorination was done by oxidising the exposed part of the silver wire in a 3M KCl solution. A current of 1 mA/cm^2 (exposed silver wire area) was sent through the silver wire to a Pt anode for 15 seconds. The current flow was repeated after changing polarity until the coating was uniform. The electrode was stored in a 3M KCl solution and kept away from sunlight.

Electrochemical characterisation by cyclic voltammetry of ferri/ferrocyanide with the Ag/AgCl electrode as working and as reference electrode gives the following results, shown in Figure B.2b until B.2d. Figure B.2b shows the stability of the electrode, Figure B.2c shows the voltammetric response at increasing voltage rates and Figure B.2d shows the (quasi-) reversibility.

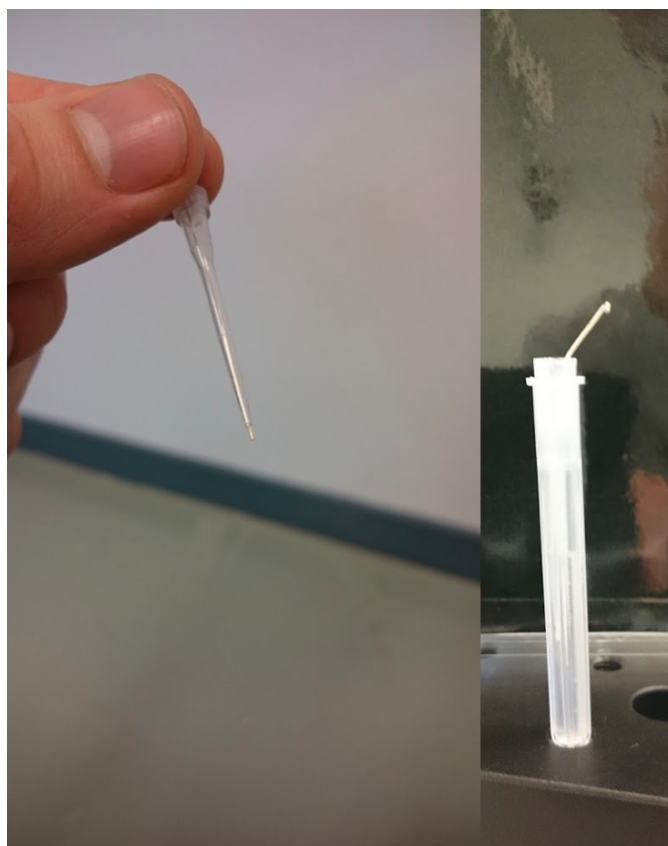


Figure B.1: Ag/AgCl reference electrode (left) and its storage container (right)

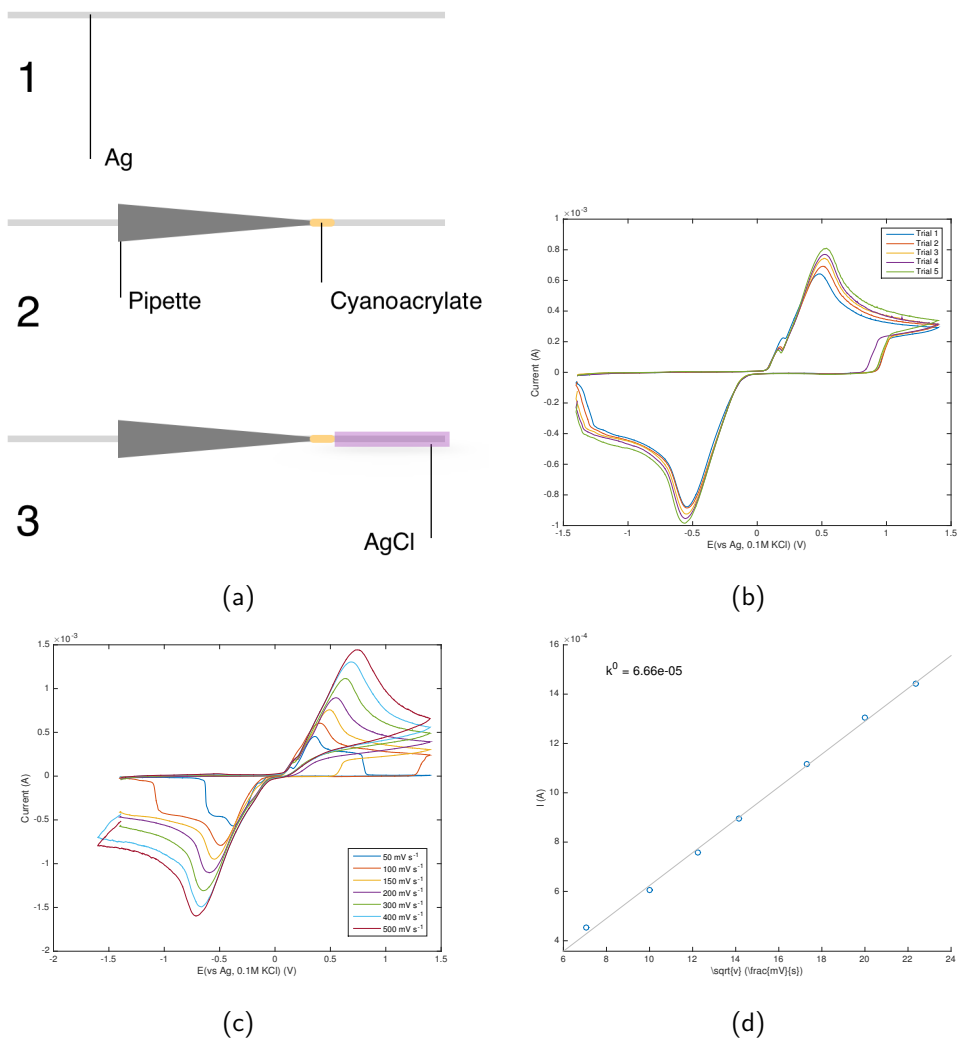


Figure B.2: **Electrochemistry of ferricyanide at a Ag/AgCl reference electrode.** (a) Steps for making the Ag/AgCl electrode (b) Repeated CVs to check electrode stability. (c) CV with different scan rates. (d) Saturated current density vs square root of scan rate. The electrolyte = 0.1 mM $K_3Fe(CN)_6$ + $K_4Fe(CN)_6$ + 0.1 M KCl

C Additional photos of CV experimental setup

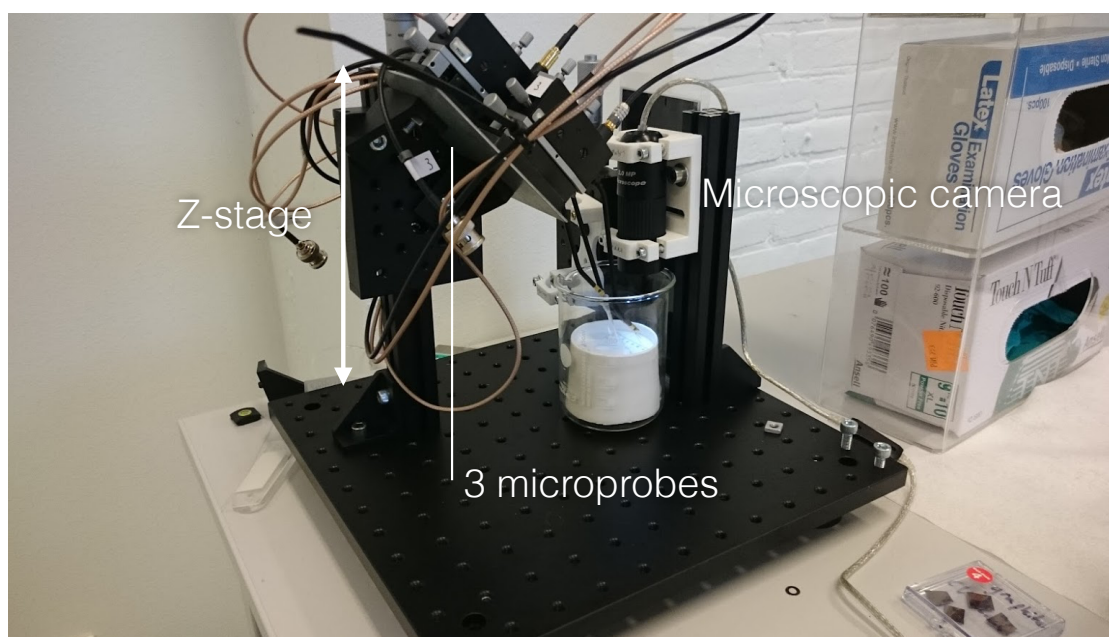


Figure C.1

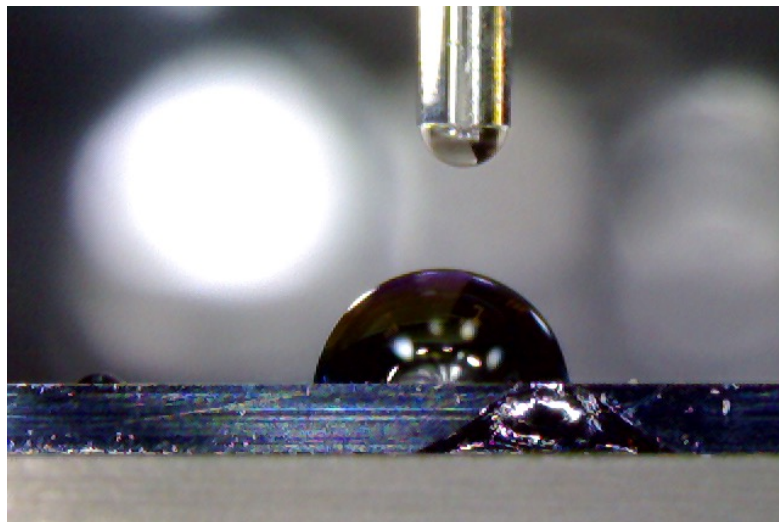


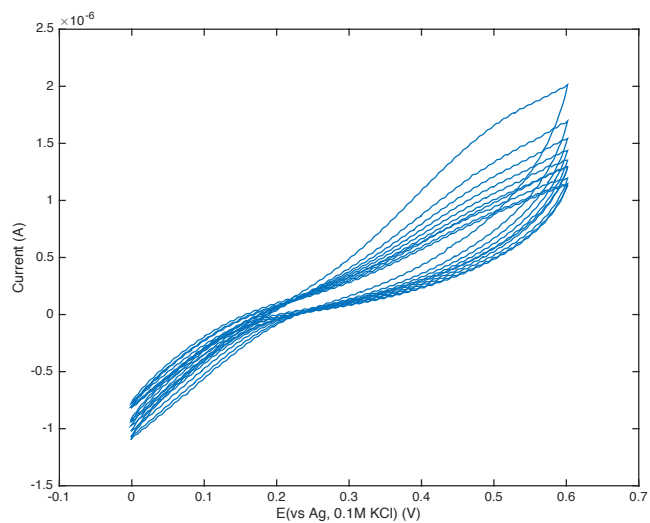
Figure C.2: Sideview droplet monitoring

D Results of the relaxed graphene CV

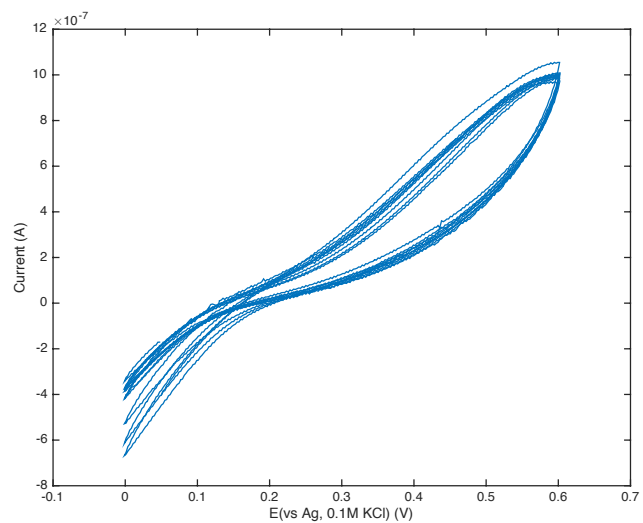
When doing cyclic voltammetry with CVD graphene as an electrode, two types of responses were recorded, of which examples are found on the following pages. The first group of responses, measured on March 3rd, didn't show any desired reactions happening between the electrode and electrolyte. At high molar levels only resistive responses are measured, at lower levels one can recognise a slow reaction happening at the electrode-electrolyte interface. A measurement done two weeks earlier, on February 24th, gave useful data that could be interpreted.

9/3/2016: CVD graphene on Si/SiO2 CV

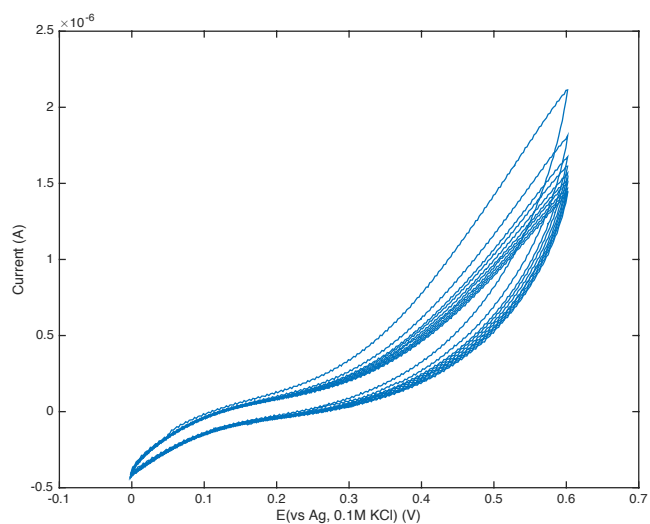
Chip 3, Ag/AgCl electrode



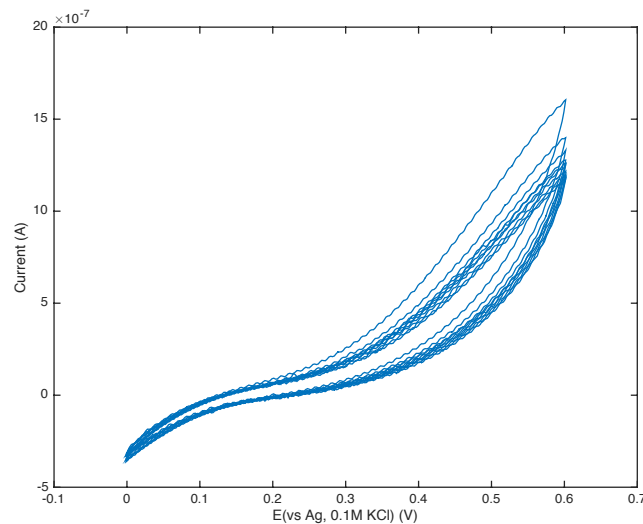
Rate = 0.1 V/s, 0.1 mM $[K_3Fe(CN)_6 + K_4Fe(CN)_6]$



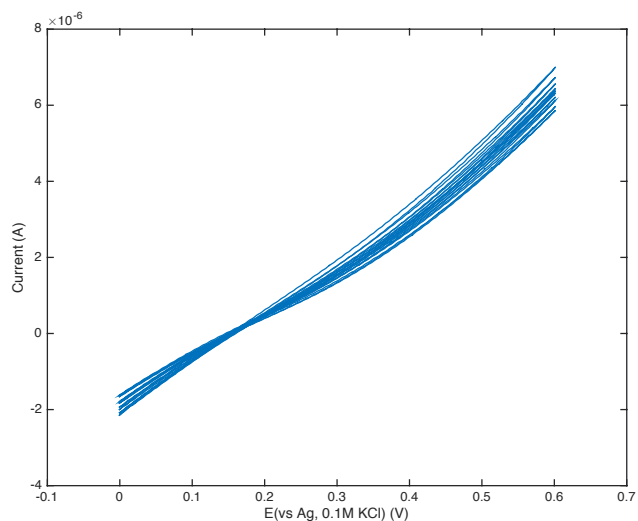
Rate = 0.05 V/s, 0.1 mM $[K_3Fe(CN)_6 + K_4Fe(CN)_6]$



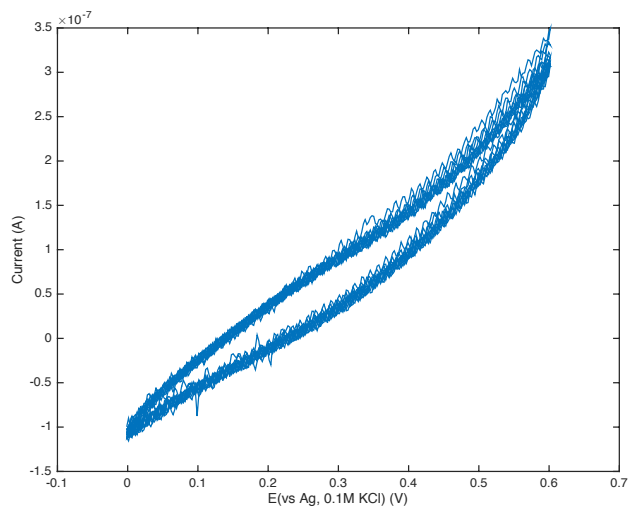
Rate = 0.2 V/s, 0.1 mM $[K_3Fe(CN)_6 + K_4Fe(CN)_6]$



Rate = 0.1 V/s, 0.1 mM $[K_3Fe(CN)_6 + K_4Fe(CN)_6]$



Rate = 0.1 V/s, 4 mM $[K_3Fe(CN)_6 + K_4Fe(CN)_6]$

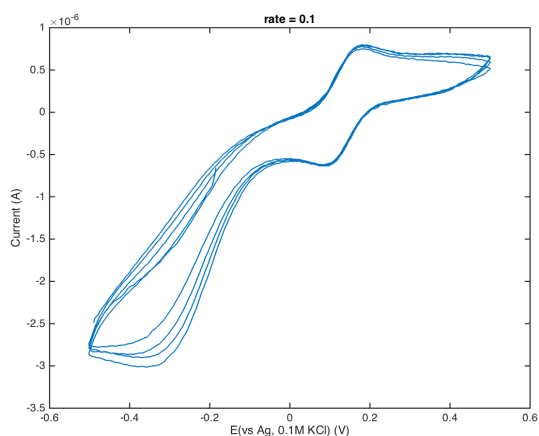


Rate = 0.1 V/s, 0.05 mM $[K_3Fe(CN)_6 + K_4Fe(CN)_6]$

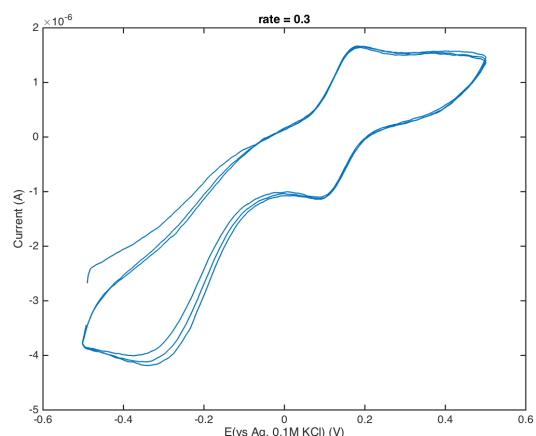
24/02/2016: CVD graphene on Si/SiO₂ CV

- Electrolyte: 0.1 mM [$\text{K}_3\text{Fe}(\text{CN})_6 + \text{K}_4\text{Fe}(\text{CN})_6$]
- Reference electrode: Ag/AgCl

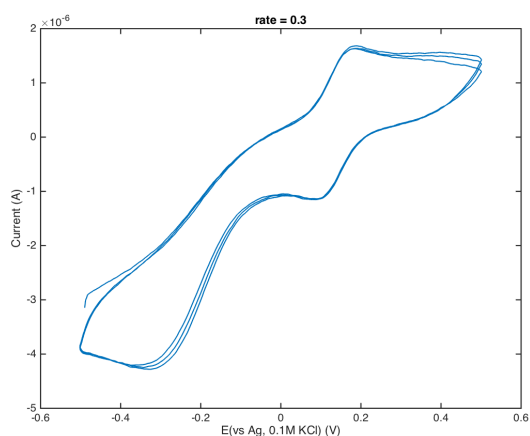
f. Rate = 0.1 V/s; 3 cycles (smoothened)



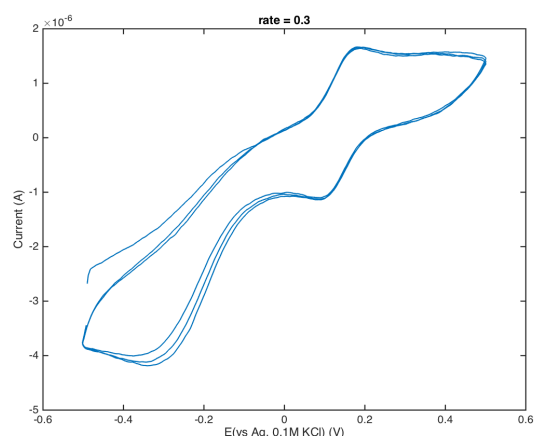
g. Rate = 0.3 V/s; ~2 cycles (smoothened)



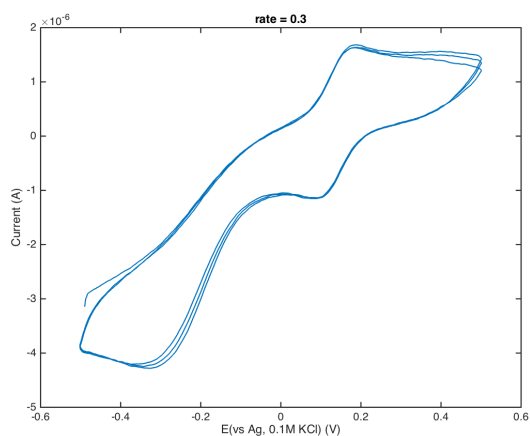
h. Rate = 0.3 V/s (smoothened)



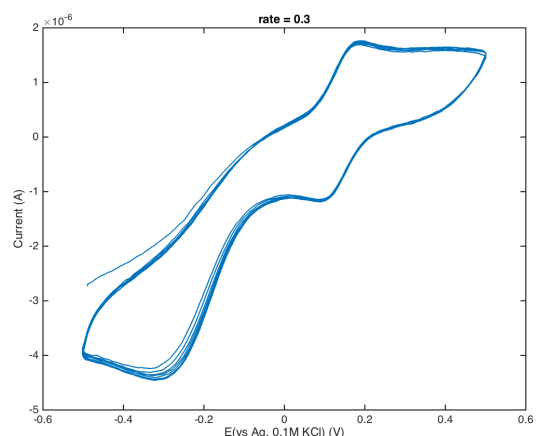
g. Rate = 0.3 V/s; ~2 cycles (smoothened)



h. Rate = 0.3 V/s (smoothened)



i. Rate = 0.3 V/s; 5 cycles (smoothened)



E Design of a micro-electrochemical cell

The ultimate test in terms of the electrochemical characterisation of strained graphene makes use of an mechanically exfoliated (ME) flake of graphene. As explained in Section 2.1, up until now, ME graphene produces the highest quality of graphene in terms of defects and grain boundaries. However, the most recent techniques have shown exfoliation of flakes in the order of $100\ \mu\text{m}$ [20], which has consequences for the electrochemical cell and wiring.

Preliminary research has been done for the development of a test setup involving electrochemical microscopy using the facilities available at the Materials Science Engineering department of 3ME at the Delft University of Technology. Unfortunately, it could not be completed, but the work done is presented here for future development.

The flexible graphene electrode is made as described in Section 4.3.2. After transfer, a Pt wire is connected to the graphene flake using Ag paint and epoxy to secure it, similar to Figure 2.10. Furthermore, the wire should be glued to the PDMS substrate at a different location to minimise stresses at the Silver-graphene connection during handling. The substrate is placed in the tensile tester as described in Section 4.

A machine-pulled (Sutter Instruments P-97) glass capillary, which can be made with a tip radius in the range of $\sim 10\ \mu\text{m}$ is inserted in a holder as shown in Figure E.1.

The holder contains a input for the counter electrode and a tube connection to the bulk electrolyte reservoir. In this reservoir a reference electrode is inserted. Between the reservoir and capillary holder, a Y tubing connector should be placed to connect a syringe, whose pressure is controlled with a syringe pump.

The capillary is positioned just above the graphene-PDMS sample and pressure is applied with the syringe pump such that a droplet is formed under the capillary and on the substrate. Now, cyclic voltammetry can be done; first when the sample is relaxed, followed by straining the substrate and repeating the experiment. The resulting voltammograms can be analysed to determine the electrochemical change of graphene upon strain.

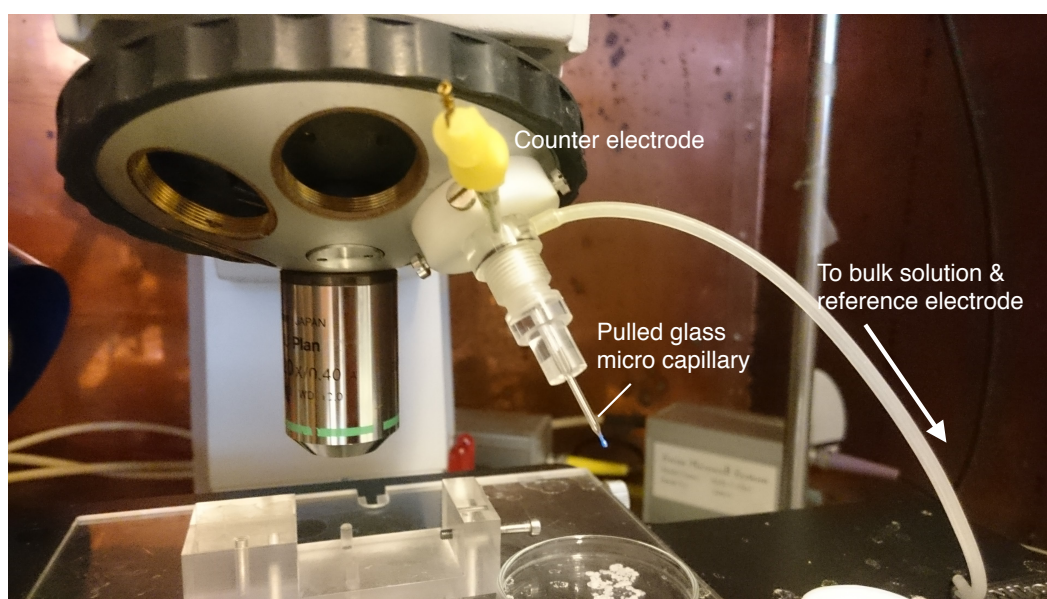


Figure E.1: Photo of the electrochemical microscopy setup